DYNAMIC CHARACTERIZATION AND ANALYSIS OF AERIAL LIFTS

A Thesis
Presented to
The Academic Faculty

by

Eileen C. Hernandez

In Partial Fulfillment
of the Requirements for the Degree
Master of Science in the
George W. Woodruff School of Mechanical Engineering

Georgia Institute of Technology
December 2012

DYNAMIC CHARACTERIZATION AND ANALYSIS OF AERIAL LIFTS

Approved by:

Dr. William Singhose, Advisor
George W. Woodruff School of Mechanical Engineering
Georgia Institute of Technology

Dr. Aldo Ferri
George W. Woodruff School of Mechanical Engineering
Georgia Institute of Technology

Dr. Joshua Vaughan
School of Mechanical Engineering
University of Louisiana at Lafayette

Date Approved: 10 October 2012

ACKNOWLEDGEMENTS

I want to thank my advisor, Dr. William Singhose, for his support and guidance. His enthusiasm of his research continues to inspire the most doubtful of graduate students and thenceforth appears constantly in their everyday life. I would also like to thank my committee members, Dr. Aldo Ferri and Dr. Joshua Vaughan, for their influence in my research through the courses they lecture and for their support of my research. I would also like to thank the GEM Fellowship for their financial support to complete a thesis for my Degree Master of Science.

I owe a debt of gratitude to my parents, Acelia and Raul, who have constantly supported my passion for engineering and running. I am blessed to have hard-working parents that have provided me great opportunities in life and help me achieve my dreams.

Lastly, I would like to thank Ehsan Maleki and Daichi Fujioka for providing assistance of this research.

TABLE OF CONTENTS

LIST OF TABLES

LIST OF FIGURES

SUMMARY

Aerial lifts are used to elevate people and material to high heights. There are many different types of aerial lifts which have vastly different dynamics characteristics. Thus, a new categorization for aerial lifts was created and organizes them by their kinematics. Many accidents occur while using aerial lifts. Hazards of aerial lifts and current solutions to those hazards were reviewed to understand the causes of the accidents. Some major accidents are due to the complex dynamics and flexibility of aerial lifts, such as oscillations and tip-overs. Oscillations of full-size aerial lifts were experimentally tested to determine frequencies in different configurations. Machine-motion induced oscillations of an articulating aerial lift were simulated and analyzed for both non-overcenter and overcenter configurations. Input shaping was used to achieve reduction in machine-motion induced oscillations. Tip-over stability margin was used to simulate and analyze the stability of both non-overcenter and overcenter configurations. The effect of increased platform mass on tip-over stability margin was also analyzed. The results in this thesis are a categorization of aerial lifts including their hazards and methods of reducing those hazards, an experimental verification of the dynamic response of full-size aerial lifts, a fully dynamic tip-over prediction model of double-boom articulating aerial lift by applying flexibility in the joints and realistic velocity profiles, and a detailed study of the dynamics of a double-boom articulating aerial lift.

CHAPTER I

INTRODUCTION

There are many ways people reach high heights to work on buildings, trees, airplanes, and other tall structures. In many cases, aerial lifts are used to provide the desired height and work environment. Aerial work lifts, like the one shown in Figure 1, provide many necessary benefits to users that need an elevated work platform. However, with those benefits come significant hazards.

> "According to the U.S. Bureau of Labor Statistics about 26 construction workers ... die each year from using aerial lifts. Approximately 70% involve boom-supported lifts, such as bucket trucks and cherry pickers; 25% of the other deaths involve scissor lifts" [1].

Figure 1: An Altec truck-mounted articulated aerial lift working on electrical lines.

From these statistical facts two main challenges can be inferred. The first challenge is determining how to reduce fatalities that occur when using aerial lifts. Therefore, there is a need to identify the most common hazards of aerial lifts and how they occur. The second challenge is understanding the different aerial work lifts (i.e. bucket trucks, cherry pickers, scissor lifts, etc.), their respective hazards, and methods to reduce those hazards. Before determining how to reduce accidents, it is important to understand the different aerial lifts well enough to develop potential solutions that could be applied to the aerial work lifts under consideration.

1.1 Description and Categorization of Aerial Lifts

Aerial work lifts have a wide range of appearances; however, all of them, are used to position people high in the air [1]. Different mechanisms are used to perform this lifting motion. The kinematic structure is what separates different types of aerial work lifts. The first distinguishing factor among aerial lifts is directionality of their motion: i) only vertical or, ii) vertical and horizontal, as shown in Figure 2. A second categorization is the method used to elevate the work platform. There are three different methods of elevation within each directional category. Vertical lifts use: i) scissor, ii) vertical mast, and iii) pulley systems. Lifts performing vertical and horizontal motion use: i) telescopic, ii) articulating, and iii) telescopic articulating. The final major way to differentiate aerial lifts is by their ability or inability to drive on the ground while elevated.

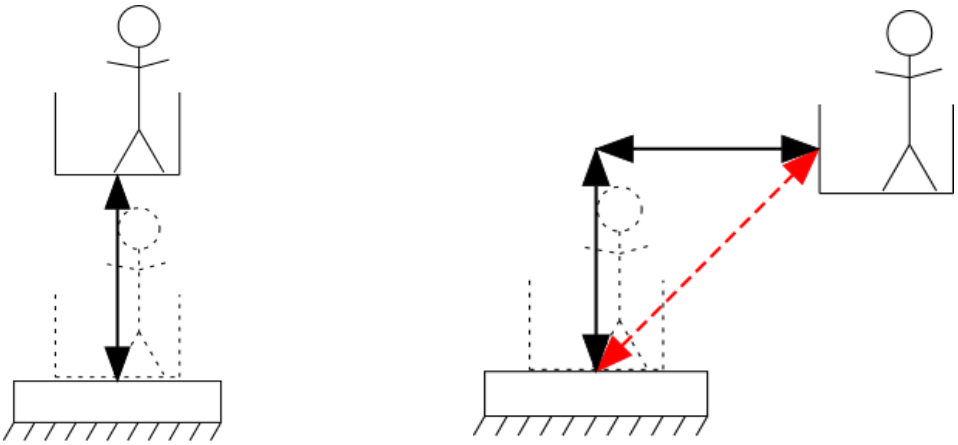

(a) Only vertical motion (b) Vertical and horizontal motion

Figure 2: Two Categories of Aerial Lift Motion.

Mobility while elevated depends on the base of the aerial lift. Lifts that are able to drive while in operation have a cab base to hold the power supply for driving. Figure 3(a) is an example of a cab-base lift. If a lift has a skeletal structure for the base or is truck-mounted, then the aerial lift is unable to drive while elevated. An example of an immobile aerial lift with a skeletal base is shown in Figure 3(b).

(a) Genie Z-80 mobile cab base telescopic articulating lift

(b) Genie TZ-34/20 immobile telescopic articulating lift with an skeletal base

Figure 3: Examples of mobile [1] and immobile aerial lifts [2].

Overall, most aerial work lifts can be placed in one of the following six classes:

1. Scissor Lifts
2. Vertical Mast Lifts
3. Pulley Lifts
4. Telescopic Lifts
5. Articulating Lifts
6. Telescopic Articulating Lifts

Scissor lifts, vertical mast lifts, and pulley lifts perform only vertical motion. Telescopic lifts, articulating lifts, and telescopic articulating lifts perform vertical and horizontal motion. Each category has variations that can or cannot drive while elevated. By including aerial lifts' mobility or immobility while elevated, the complete categorization of aerial lifts is given in Table 1.

[1] http://www.genielift.com/en/products/new-equipment/boom-lifts/index.htm
[2] http://www.genielift.com/en/products/new-equipment/trailer-mounted-booms/index.htm

Table 1: Categorization table of aerial work lifts.

	Vertical Lifts		
	Scissor Lift	**Vertical Mast Lift**	**Pulley Lift**
Mobile while Elevated	 3	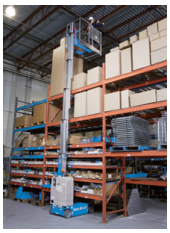 4	
Immobile while Elevated	 5	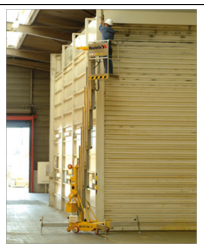 6	 7

	Vertical and Horizontal Lifts		
	Telescopic Lift	**Articulating Lift**	**Telescopic Articulating Lift**
Mobile while Elevated	 8	 9	 10
Mobile while Elevated	 11	 12	 13

[3]http://www.genielift.com/en/products/new-equipment/scissor-lifts/slab-scissor-lifts/gs1530/index.htm
[4]http://www.genielift.com/en/products/new-equipment/vertical-mast-lifts/runabout/index.htm
[5]http://www.snorkellifts.com/PR_TrailerScissor.aspx
[6]http://www.haulotte-usa.com/access_equipment-ELV-EN.htm
[7]http://www.liftpod.com/en-US/Home.html, JLG-LiftPod-Aerial-Work-Platform-Brochure.pdf
[8]http://www.genielift.com/en/products/new-equipment/boom-lifts/telescopic-booms/index.htm
[9]http://www.genielift.com/en/products/new-equipment/boom-lifts/index.htm
[10]http://www.genielift.com/en/products/new-equipment/boom-lifts/index.htm
[11]http://www.elliottequip.com/products/hireach-aerial-work-platform/hireach-models/2011/11/17/i50f
[12]http://www.genielift.com/en/products/new-equipment/trailer-mounted-booms/tz3420/index.htm
[13]http://www.terexutilities.com/en/products/new-equipment/overcenter-aerial-devices/index.htm

The power supply used by aerial lifts does not depend on the directionality of its motion. It depends on the intended work environment. Two different work environments for aerial lifts are: i) indoor and ii) outdoor environments. Indoor environments restrict the power supplies to those that do not emit exhaust such as electric, manual, battery, and sometimes a hybrid that uses gas or diesel outdoors and electricity or battery indoors. Outdoor environments are not as restrictive as indoors; thus, all power supplies can be used. Other options that apply to all aerial lifts are insulation for electrical work and/or reinforced heavy duty for industrial work.

Some companies that are well known for aerial work lifts include: Terex, Niftylift Altec, JLG, Haulotte, Reachmaster, Skyjack, Snorkel, Elliot, Versalift, MLE Man Lift Manufacturing Co., and Hi-Reach. MLE Man Lift Manufacturing Co. specializes in making custom aerial lifts such as clean room lifts and pedestal mount man-lifts. Bridge Across Specialties, West Coast Under Bridge Platforms, and Palfinger specialize in truck-mounted aerial work lifts capable of accessing beneath bridges for repair, maintenance, and inspection, as shown in Figure 4.

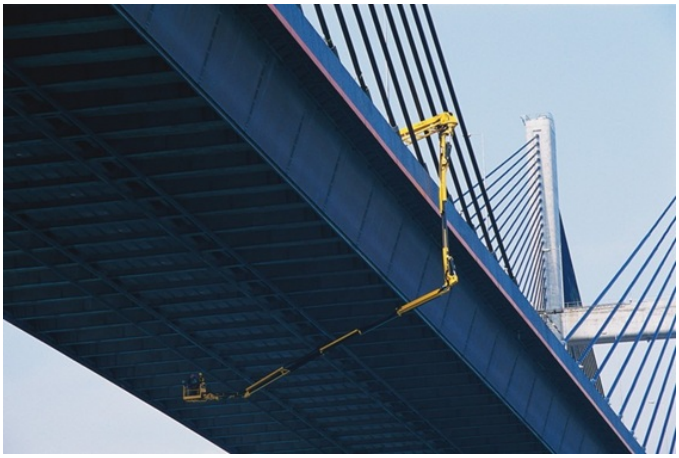

Figure 4: Palfinger's vehicle-mounted bridge inspection lift performing maintenance under a bridge. [14]

[14]https://www.palfinger.com/en-US/usa/products/

1.1.1 Vertical Lifts

Vertical lifts are split into three subsections: scissor lifts, vertical mast lifts, and pulley lifts. Scissor lifts are identified by their unique structure that resembles multiple scissors retracting to reduce height and expanding to increase height, as seen in Figure 5.

Figure 5: Genie GS-1530 scissor lift with cab base.[15]

Vertical mast lifts have multiple sections that either fit inside one another or equal sections that slide up against one another to increase height. An example of a vertical mast lift is shown in Figure 6. Both scissor lifts and vertical mast lifts have the option of mobility while elevated. If the lift has a cab base, like the one in Figure 5, then the lift can drive while elevated.

Pulley lifts use the common pulley system to elevate the location of the working platform. Currently, the only known pulley lift available has a skeletal structure for a base. A pulley lift cannot be mobile while elevated because it has a skeletal structure for a base, as shown in Figure 7.

All vertical lifts can be used outdoors. Due to the small bodies and footprints of vertical lifts, they can also all be used indoors as long as they are not gas or diesel powered.

[15] http://www.genielift.com/en/products/new-equipment/scissor-lifts/index.htm

Figure 6: Haulotte immobile vertical mast lift.[6]

Figure 7: JLG's Liftpod that uses a pulley system.[7]

1.1.2 Vertical and Horizontal Lifts

Vertical and horizontal lifts are comprised of: articulating lifts, telescopic lifts, and telescopic articulating lifts. All vertical and horizontal motion aerial lifts achieve lifting by pivoting their boom(s), represented as a dashed red line in Figure 2(b). The booms of a vertical and horizontal aerial lift are commonly referred to as the arm of the aerial lift. In addition, vertical and horizontal motion aerial lifts rotate at the base to provide access in all directions.

Figure 8(a) shows a rotation at the base around the vertical axis of an aerial lift commonly referred to as a slew movement. Figure 8(b) shows a rotation around a horizontal axis of an aerial lift commonly referred to as a luffing movement, which is the result from pivoting their booms.

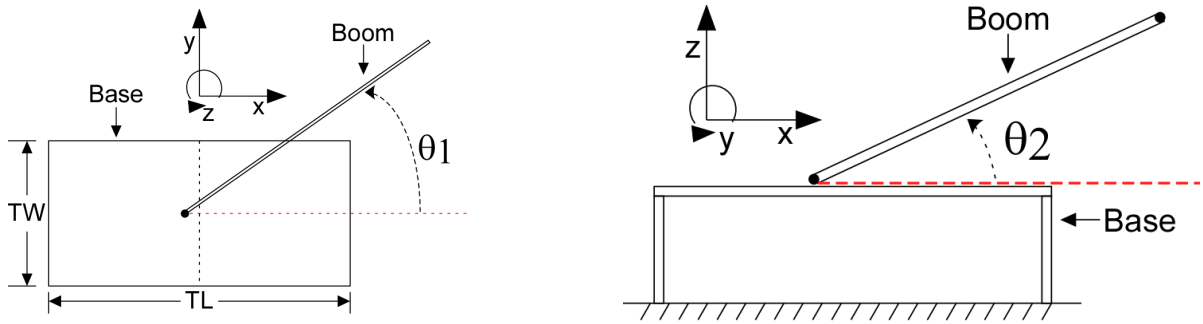

(a) Slewing motion (overhead view)

(b) Luffing motion (side view)

Figure 8: Movements of vertical and horizontal motion aerial lifts.

An articulating aerial lift has two or more hinged boom sections that pivot at the hinges to elevate the working platform [1]. Figure 9 shows a truck-mounted articulating aerial lift with multiple boom sections.

Figure 9: Altec articulating aerial lift.

Aerial lifts with only one hinged boom section may be telescopic lifts or just a one boom aerial lift. Telescopic lifts can slew, luff, and their boom length can increase due to the

Figure 10: Genie S-60's Trax cab base telescopic aerial lift. [16]

multiple sections within a boom. The cab-mounted telescopic lift in Figure 10 has a smaller section extending out of the top part of the boom to increase the boom length.

Telescopic articulating aerial lifts are articulating lifts and telescopic lifts combined. Telescopic articulating lifts have multiple hinged boom sections, can slew, luff, and their booms can increase in length. Figure 11 shows an aerial lift with multiple booms and its upper boom can expand in length due to the telescopic sections.

Figure 11: Genie Z-60/34 cab base telescopic articulating lift. [10]

Vertical and horizontal lifts can be mobile or immobile while elevated depending upon the base of the aerial lift. Vertical and horizontal aerial lifts have three base options:

[16] http://www.genielift.com/en/products/new-equipment/boom-lifts/telescopic-booms/index.htm

Figure 12: Genie TZ-50 is a skeletal base telescopic articulating lift. [17]

skeletal, cab-mounted, or truck-mounted. Skeletal base aerial lifts cannot drive while raised. However, they can be used in indoor or outdoor environments, as shown in Figure 12.

Truck-mounted aerial lifts cannot be mobile while raised. In addition, truck-mounted aerial work lifts are not an option for indoor environments due to restricted access and exhaust created by internal combustion engines. Truck-mounted aerial work lifts are commonly used for outdoor applications. A truck-mounted aerial lift that has two articulating booms is commonly known as a cherry picker, as shown in Figure 13. Cherry pickers were first used primarily in orchards to pick fruits because they could easily elevate and rotate operators to the side of the truck, allowing quick access to the produce. Similar to produce in orchards, electrical lines and telephone poles span long distances at elevated heights. Therefore, cherry pickers are also commonly used by electrical companies for routine checkup, maintenance, and repair of power lines, especially after damages occur from a storm. Some companies that make truck-mounted aerial work lifts in the United States are: Altec, Terex, Elliot's Hi-Reach, and Versalift.

From truck-mounted aerial lifts came the smaller aerial lifts supported by a cab base

[17] http://www.genielift.com/en/products/new-equipment/trailer-mounted-booms/index.htm

Figure 13: An elevated cherry picker.

Figure 14: A cab-mounted aerial lift used to perform work on a building at MIT.

instead of a truck [18]. Cab-mounted aerial lifts can be driven while raised. Cab-mounted aerial lifts can be used outdoors and some cab-mounted aerial lifts are also capable of fitting through doorways for indoor usage. An example of a cab-mounted aerial work lift is shown in Figure 14. Some companies or brand names that make cab-mounted aerial work lifts in the United States are: Genie, which is owned by Terex, JLG, Haulotte, Reachmaster, Skyjack, and Snorkel.

[18] http://www.versalifteast.com/articles/evolutionliftindustry.htm

The range of motion for booms of articulating aerial lifts vary greatly from one lift to another. In general, articulating lifts with additional boom range of motion are identified as overcenter (OC) as opposed to non-overcenter (NOC) aerial lifts. Non-overcenter refers to the joints' ability to only reach a maximum of 90° from horizontal for the lower boom and a maximum of 180° from horizontal for the upper boom. A non-overcenter aerial lift's allowable motions are illustrated in Figure 15. In Figure 15, the base of the aerial lift is portrayed as a gray box, the lower boom is a continuous red line, previous positions of the lower boom are dashed red lines, the upper boom is a continuous blue line, previous positions of the upper boom are dashed blue lines, and the payload is a yellow circle. The first configuration in Figure 15 is a compact aerial lift, which is the typical orientation of lifts before operation. The second configuration shows the upper boom luffed 90° from the lower boom. The third configuration is the lower boom luffed to it's maximum angle of 90°. The last configuration shows how the upper boom can luff an additional amount to reach its maximum angle of 180° from the lower boom.

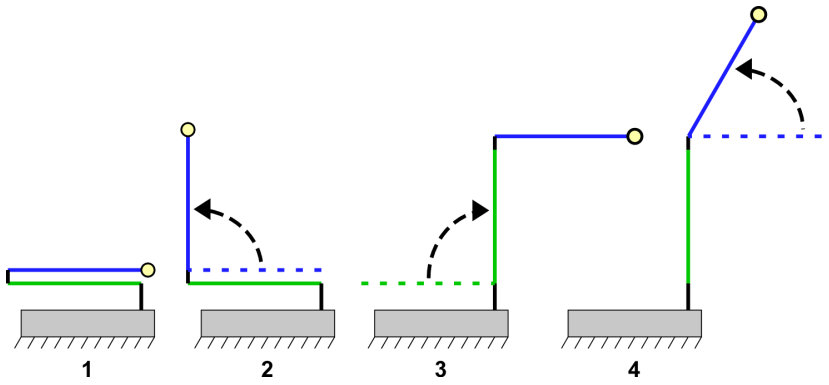

Figure 15: Non-overcenter articulating aerial lift allowable motions.

Overcenter refers to the ability of the joints to reach past 90° from horizontal for the lower boom and/or past 180° from horizontal for the upper boom[19]. An overcenter aerial lift's motions are illustrated in Figure 16. Obviously all overcenter aerial lifts are non-overcenter aerial lifts, because they can perform non-overcenter configurations, as well. However, only truck-mounted non-telescopic articulating aerial lifts can have overcenter abilities due to restrictions from the telescoping boom sections. The first configuration in Figure 16 shows the aerial lift in compact form. Then, the upper boom luffs past 180° from

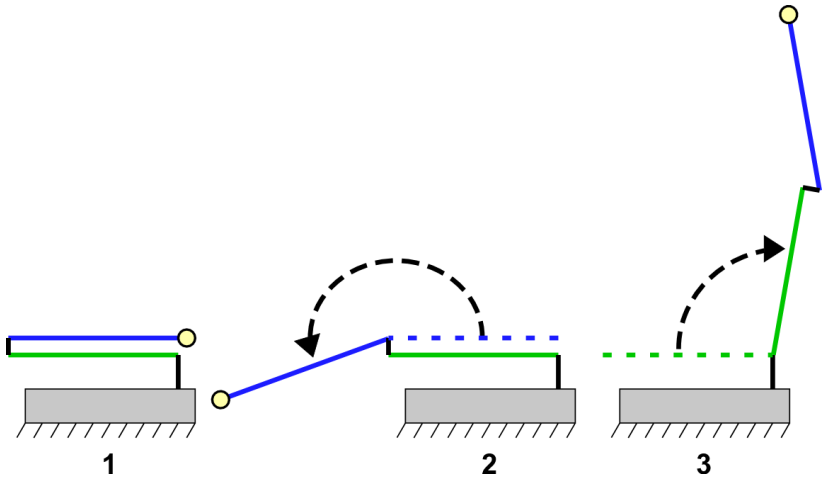

Figure 16: Overcenter articulating aerial lift allowable motions.

the lower boom, the limit for non-overcenter aerial lifts. In the last configuration, the lower boom luffs past 90° from horizontal, the limit for non-overcenter aerial lifts.

A summary of the motion constraint for an overcenter and non-overcenter aerial lift are shown in Table 2.

Table 2: Overcenter and non-overcenter constraints.

	Lower Boom Angle	**Upper Boom Angle**
Non-Overcenter	90°	180°
Overcenter	90+°	180+°

1.1.3 Hazards of Aerial Lifts

For many construction and utilities jobs, aerial lifts are used to reach extremely elevated locations. At elevated locations there are many risks to the operators in the platform. Different aerial lifts have different degrees of risks and methods for reducing those risks. To explain the degree of hazards, terminology must first be defined. First, a hazard can be defined by its severity to the operator: catastrophic, critical, marginal, or negligible. Catastrophic means the hazard will most likely result in death; critical is when large body parts are injured; marginal is when a part of the body is strained or small injuries occur that can be treated with bandages and wraps; and negligible is when little to no physical injury

[19] http://utilityequipment.blogspot.com/2006/06/over-center-vs-non-over-center.html

occurs. Second, a hazard can be defined by the probability of the hazard occurring: frequent, probable, occasional, or unlikely. Frequent means the hazard has the greatest probability of occurrence; probably has the second highest probability of occurrence; occasionally has the second smallest probability of occurrence; and unlikely is an accident that has the smallest probability of occurrence. This risk assessment is a first-order general assessment to further describe the risks when using aerial lifts and detail ways to reduce those risks.

Common aerial lift hazards can be grouped into eleven different events: electrocution, tip-over, reach fall, auto collision, crushing, power failure, unleveling of platform, falling tools or supplies, oscillations, obstacle collision, and acrophobia. The most severe and common occurring hazard is electrocution of the operator in the aerial lift platform. Over one-third of the electrocutions involved an overhead power line contacting the lift boom or bucket [1], resulting in death because of the high current in power lines. Electric shocks, in comparison, are caused by lower currents that do not result in death. Given that many aerial lifts are used by electrical companies to maintain electrical lines that run high above ground, as shown in Figure 17, electrocution has an occasional probability of occurring. Vertical and horizontal aerial lifts experience the most electrocutions because they are capable of easily rotating toward the power lines.

Figure 17: A truck-mounted aerial lift working on power lines.

Another catastrophic event that happens occasionally is falling from the aerial lift while standing on or leaning over railings of the platform to reach for an item [1]. Reaching out and falling from a lift can occur in any lift, especially if the magnitude of the force exerted is large. However, most reach falls occur in vertical and horizontal aerial lifts because their platforms are less supported than vertical lifts. The least likely catastrophic hazard on aerial lifts is an auto collision. Auto collision is when another vehicle strikes the lift, usually resulting in the operator being ejected from the bucket [1]. Auto collisions can happen to any aerial lifts as long as the lift is in close vicinity to other vehicles. Aerial lifts are close to other vehicles when they are on construction sites and especially when they are on roadways. Truck-mounted aerial lifts are typically on roadways; thus, they are more likely to be in auto collisions.

For the majority of aerial lifts, tip-over/collapse was the most common event, 56% in scissor lifts and 44% in boom lifts [15]. Tip-over is another catastrophic event that has an occasional probability of occurring and can happen on any aerial lift. For scissor lifts, three-quarters of the reported tip-overs resulted in fall deaths and about two-fifths occurred when the scissor lift was extended over 15 feet, mostly while driving the lift [1]. Tip-overs, as shown in Figure 18, result from instability due to the center of mass lying outside of the support base; however, many different events can cause instability to occur:

- Mechanical or structural failure
- Exceeding load limits
- Damp, sloped, or unstable grounds
- Large forces from obstacles or wind
- Oscillations

For articulating aerial lifts, statically unstable configurations can also cause tip-overs to occur.

Keeping track of all the components of an aerial lift is difficult, while maneuvering it from the platform situated at the top. Thus, colliding with an object has a probable probability

[20] "UPDATE: Child released from hospital, uncle recovering after bucket truck accident in South Bend", Jeff Harrell, http://articles.wsbt.com/2011-06-24/bucket_29701244.

Figure 18: A tipped over aerial work lift.[20]

of occurring. As long as the aerial lift does not tip-over or the operator get ejected from the platform, colliding with an object produces marginal injuries unless the aerial lift is in close vicinity electrical lines; thus, electrocution can occur. All aerial lifts can experience obstacle collisions; however, articulating aerial lifts, especially telescopic articulating aerial lifts, are more likely to collide with obstacles because they have the most variably-positioned parts of any other aerial lift. For scissor lifts, the occasional fall due to an object strike occurs as well. A more serious form of collision is when the operator is crushed or caught between the bucket edge and objects such as, roof joists or beams, while repositioning the bucket [1]. Crushing, as illustrated in Figure 24, is a critical hazard that occasionally occurs. Any aerial lifts can have their operator caught between the platform and an obstacle; however, articulating aerial lifts are more likely due to their complex positioning capabilities.

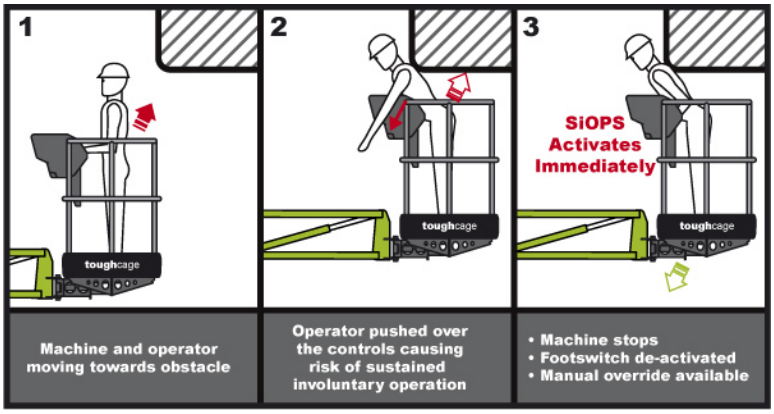

Figure 19: Hazard of an operator crushed between the control panel and an obstacle.[23]

When operating any aerial lift, the system's flexibility induces oscillation. Oscillations on their own do not result in catastrophic accidents. Oscillations, which occur frequently, could cause nausea. However, oscillations in the close vicinity of objects, such as electrical lines, could cause electrocution, the operator to fall from colliding with an obstacle, or the aerial lift to tip-over, which are all catastrophic accidents. From previous research, it is known that articulating aerial lifts' movements induce large and dangerous oscillations in luffing and slewing motions [20] due to the lift's long, flexible booms. In addition, there are larger oscillations when the platform is carrying more weight [17]. Articulating lifts also have larger oscillation when the booms are in an extended configuration compared to a compact configuration. Extended configurations also have a longer settling times due to the platform's inertia creating larger oscillations [10].

Power failure usually occurs to aerial lifts running on batteries/electricity because of either the battery running out of power or a local power failure knocking out the electricity. Power failures can also occur in aerial lifts that run on diesel or gasoline; however, typically operators can tell when those resources are low. Results from a power failure can be critical, unless preventive measures are taken. In some aerial lift designs, holding the platform elevated requires power. Given that aerial lifts need a power supply at each use, power failures are a probable hazard.

A hazardous event that happens frequently is an operator dropping their tools or supplies. All aerial work lifts are meant for workers who typically need various tools to do their job. Each aerial lift has some form of tool tray, although that does not stop the common occurrence of an operator dropping his/her tools. Injuries resulting from dropping one's tools has a marginal probability given the small likelihood of a person passing underneath when the event occurs.

Unleveled platforms are not likely to occur as long as the aerial lift is working properly, although the hazard is more common on vertical and horizontal aerial lifts due to their less supported platforms, as shown in Figure 20. Typically, vertical and horizontal aerial lifts have platforms supported by a beam connected to the highest boom, while vertical lifts

[23] http://www.niftylift.com/usa/news/focus-on/siops-sustained-involuntary-operation-prevention-system

are almost always supported by their elevating structure. Fortunately, a slight mis-leveling does not usually cause catastrophic results. It is a critical event if the operator is unable to return to ground before resulting in a complete structural failure causing the operator fall to the ground.

Figure 20: Altec AT237 articulating aerial lift showing the less supported platform.[21]

The last hazard of aerial lifts, which has a negligible severity, is acrophobia, the fear of heights. Acrophobia is a mental reaction that is negligible unless a physical action is taken to counteract the fear. Fear of height occurs frequently on any aerial lifts; however, greater fear of height usually happens at higher heights. Thus, acrophobia commonly occurs on telescopic aerial lifts.

Hazards of articulating aerial lifts are summarized in Table 3. Hazards with the greatest severity and largest probability of occurrence are at the top left, while hazards with the least severity and fewest occurrences are at the bottom right. Some hazards, such as electrocution cannot change in severity; however, the probability of many risks can be changed by utilizing the many different possible designs for aerial lifts.

[21] http://www.altec.com/aerials.php

Table 3: Risk assessment for articulated aerial lifts.

		Probability			
		Frequent	**Probable**	**Occasionally**	**Unlikely**
Severity	**Catastrophic**			Electrocution, Tip-Over, Reach Fall	Auto Collision
	Critical		Power Failure	Crushing	Unleveled Platform
	Marginal	Drop Tools, Oscillations	Obstacle Collision		
	Negligible		Acrophobia		

1.1.4 Reduction of Hazards

Aerial lifts hazards can be reduced by both daily practices and/or mechanical options. Electrocution is a common hazard that can be resolved by the operators. To avoid electrocution, operators should rent/purchase insulated aerial lifts and wear electrical clothing protection at all time while in the aerial lift. To ensure safety from electrocutions, if possible all nearby overhead power lines should be turned off before beginning work.

Tip-overs on an aerial lift can be prevented by as many ways as the hazard can be caused. A set slope limit for each aerial lift is a way to ensure sloped surfaces do not cause tip-overs. In addition, most aerial lifts have base level indicators to warn operators, if the surface's slope is greater than the safe limit. Along with a slope limit, each lift has a platform load capacity because the platform's weight greatly contributes to the location of the aerial lift's center of mass.

Besides limiting certain aspects of what aerial lifts can handle, many mechanical features on aerial lifts can also prevent tip-overs. The majority of aerial work lifts have outriggers used to increase the range of stability, increase the reach, and level the aerial work lift. Outriggers are an extendable axle that expands the support base to enhance the vehicle's stability allowing the center of mass wider area of stable locations [18]. There are two common types of outriggers. An A-frame outrigger pulled out from the vehicle pedestal and typically spreads to 8 ft. An example of this outrigger is shown in Figure 21(a). An MH type out-and-down outrigger typically spreads to 18 ft. An example of this outrigger

is shown in Figure 21(b). Most outriggers are equipped with check valves, thermal-relief valves, and separate operating controls for each outrigger for safety purposes [22]. Hydraulic or manual stabilizers also help keep the aerial lift level. If a lift's outriggers are not setup and an aerial work lift's center of mass moves over the support base, then the lift could tip-over. Both types of outriggers can be combined on one lift, as shown in Figure 22. Aerial lifts that can drive while the platform is elevated, cannot use outriggers while driving.

(a) Aerial lift with an "A-frame" outrigger.

(b) Aerial lift with "MH" outrigger.

Figure 21: Different types of outriggers used to stabilize aerial lifts.

Figure 22: Aerial lift with both outrigger types.[22]

Many aerial work lifts also have interlocks. Interlocks are used differently in different

[22] http://www.elliottequip.com

types of aerial lifts; however, their general purpose is to control the use of an operation to provide further stability. Some Interlocks are used to prevent the use of drive and steer functions while raising the boom. Other interlocks are also used to make sure outriggers are in place before lifting the platform. However, there have been cases of interlock systems malfunctioning and resulting in accidents [18].

From previous research on two boom articulating lifts, with the rotating tower located longitudinally closer toward one end of the base, static tip-over was shown to more likely occur with the extended booms of the aerial lift over the rotating tower end of the base, as shown in Figure 23 labeled 3 [4]. Another likely static tip-over position is with the extended booms parallel with the cherry picker's lateral axis, the sides of the aerial lift, as shown in Figure 23 labeled 1 and 2. When the joint angles increase into a more compact form, the static tip-over possibility decreases [4].

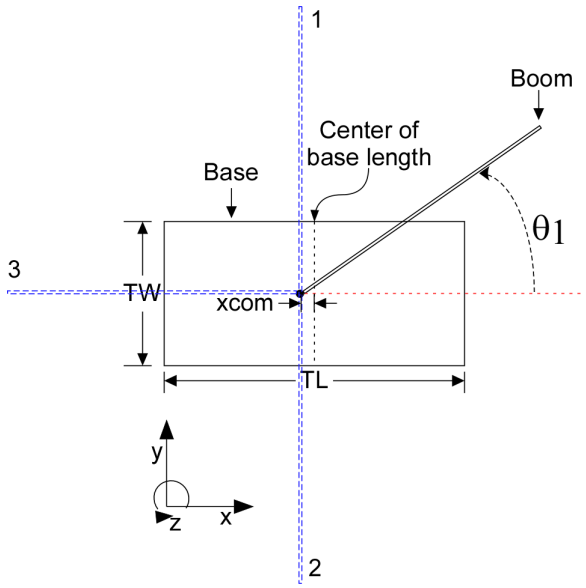

Figure 23: Configurations with greater probability of tip-over on articulating lifts.

To protect operators from reach falls, there are guidelines. First, operators should remember to wear a full-body harness and lanyard connecting them to the aerial lift's platform. Second, operators must never climb or stand on platform railings or sides to complete work. Operators should always get close enough to their elevated work site and equipment to not have to reach far over the platform edges. In addition, the aerial lift

should be repositioned each time the elevated work location changes helping to ensure a minimum distance to the targets and safety from reach falls.

Auto collision accidents can be avoided by posting up work zone warnings around the aerial lift and any space intended for use of driving the aerial lift. If the driving function is not to be used while elevated, then the outriggers of the aerial lift could be set up to provide an extra guard against impacting the aerial lift. In addition, operators should also wear a full-body harness and lanyard connecting themselves to the platform of the aerial lift to prevent them from falling to the ground after an auto collision ejects them from the platform.

Solutions to oscillation resulting from movements of an aerial lift are currently unavailable in most cases. The only solution to reducing the hazards of oscillations is limiting the speed of the aerial lift as it lifts and rotates the platform and limiting the speed of the driving motion. Obstacle collisions are also quite unavoidable, except by reducing speeds to reduce overshooting the desired end location and colliding with the target.

A couple of mechanical solutions exist to prevent crushing accidents. By adding a kill switch to the control panel to shut down the system at the last location, operators can prevent the aerial lift from reaching a crushing position. In addition, warning signals are sometimes associated with the kill switch to notify workers in the vicinity of the distressed operator in the aerial lift. Then, workers on the ground can use the control panel located at the base of the aerial lift to take over control of the lift. Other times, the platform control panel can have an end operation switch, which can sense if the operator is caught between the control panel and another obstacle, as shown in Figure 24.

Power failure accidents are greatly diminished due to lock valves that can hold a lift at the last configuration before power failure; thus, the aerial platform will not fall to the ground. Many aerial lifts also have the option for manual descent in case of a power failure. Therefore, the operator can safely return to the ground unharmed. Most importantly, most aerial lifts have low power supply warnings to alert operators before a power failure. Areial lifts equipped with all these measures should rarely experience power failure accidents.

[23]http://www.niftylift.com/usa/news/focus-on/siops-sustained-involuntary-operation-prevention-system

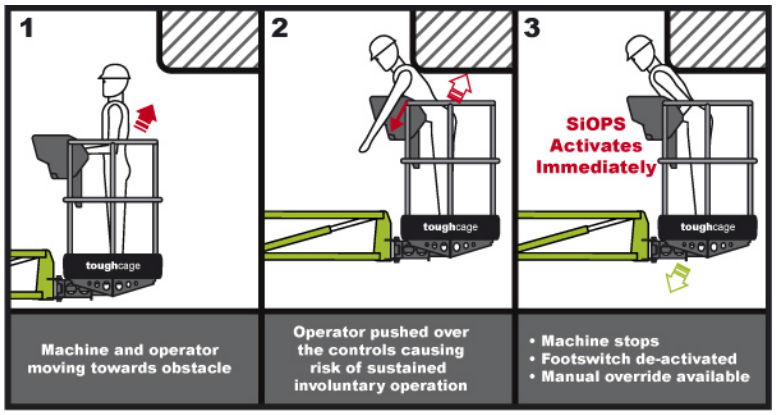

Figure 24: Solution to hazard of an operator crushed between the control panel and an obstacle.[23]

Dropping tools is a common occurrence that can decrease in severity by operators holding on to their tools and posting restricted access signs around the aerial lift work site. Tool trays inside of most aerial lift platforms should also have their own straps to secure tools while the aerial lift is in motion and the tools are not in use. In addition, tools themselves should have a lanyard connecting them to the platform or operator's wrist, as long as the lanyard does not take away function from the tool or obstruct operators from their work.

Unleveled platform accidents are prevented by self-leveling platforms and a platform level indicator, instead of just a base level indicator. In addition, inward opening gates on platforms could help in unleveled platform accidents compared to outward opening gates by preventing accidental opening of the gates, making the situation worse.

Acrophobia is a hazard without much of a solution because it is mental. To take away the view of the height is impossible and would interfere with moving the aerial lift. Simply getting used to the view or to not look down often could reduce acrophobia.

1.2 Input Shaping

One mechanism to reduce undesired oscillation of flexible systems is by input shaping. Input shaping uses measurements of the system's states to alter the shape of either actuator commands or set points [19]. Although shaping a system's commands costs time, the time is small compared to the time saved in waiting for settling of the machine's oscillation [19]. To implement a simple input shaper, the frequency and damping ratio of a oscillation must be

calculated to determine the impulses and time for the impulses to occur. After determining the impulses and time stamps of the input shaper, it is convolved with a desired system input command to create a shaped input, as shown in Figure 25.

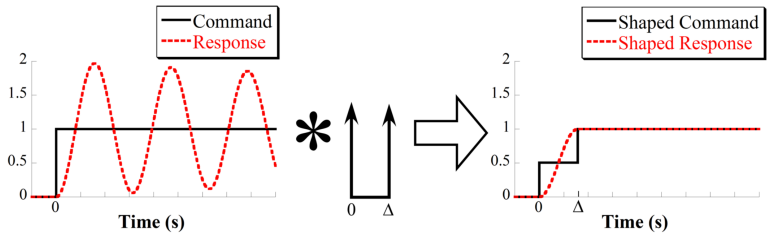

Figure 25: Input shaping

One basic input shaper is the ZV shaper which has the following form:

$$\mathbf{ZV} = \begin{bmatrix} A_i \\ t_i \end{bmatrix} = \begin{bmatrix} \frac{1}{1+k} & \frac{k}{1+k} \\ 0 & \frac{\tau_d}{2} \end{bmatrix} \tag{1}$$

Where τ_d is the damped oscillation period and $k = e^{\frac{-\zeta\pi}{\sqrt{1-\zeta^2}}}$.

1.3 Thesis Contributions

The major contributions of this thesis are:

- A categorization of aerial lifts including their hazards and methods of reducing those hazards
- An experimental verification of the dynamic response of full-size aerial lifts
- A fully dynamic tip-over prediction model of double-boom articulating aerial lifts by applying flexibility in the joints and realistic velocity profiles
- A detailed study of the dynamics of a double-boom articulating aerial lift

1.4 Thesis Outline

Chapter I categorized aerial lifts by their kinematics. In addition, the severity and frequency of aerial lift hazards were investigated.

Chapter II presents experimental results from life-size scissor lift and articulating aerial lift. Machine-motion and operator induced oscillations on a scissor lift are conducted and analyzed. Machine-motion induced oscillations on an articulating aerial lift is analyzed.

Chapter III studies the dynamics for a double-boom articulating aerial lift. A dynamic model of a double-boom articulating aerial lift is simulated and its oscillations induced by different moves and configurations are analyzed. Input shaping is used to reduce oscillation.

In Chapter IV, the dynamic model of an articulating aerial lift and a tip-over stability margin are used to investigate stability at different configurations and with varied platform mass.

Chapter VI provides concluding remarks and future work.

CHAPTER II

FULL-SIZE AERIAL LIFT OSCILLATION EXPERIMENTS

From the categorization of aerial lifts and their hazards presented in Chapter 1, it is clear that further investigation into methods of reducing hazards is necessary. There are two significant physical properties of aerial lifts that contribute to hazards i) oscillations of the structure and ii) tip-over instability. Oscillations of aerial lifts lead to many other risks, such as colliding into objects and electrocution; thus, it should be studied to determine how to reduce the risk. In this chapter, some aerial lifts were experimentally tested to measure the amount of oscillation induced by common motions performed by the aerial lifts. Two scenarios that generate oscillation are i) moving the machine's location and ii) forces the operator induces while working on the platform.

2.1 Scissor Lift Oscillations

2.1.1 Machine-Motion Induced Oscillations

For a scissor lift, machine-motion induced oscillations are a cause for concern and discomfort to operators. To demonstrate these types of oscillations caused by movement of a scissor lift, the scissor lift shown in Figure 26 was raised and its movement was recorded with a camera during a vertical drop. The scissor lift uses battery power to operate and was made by UpRight, now Snorkel, company. It has a maximum capacity of 454 kg, a maximum height of 7.93 m, and a platform of dimensions 1.22 m in width by 2.29 m in length.

Figure 27 shows the maximum residual vertical oscillation of 10 mm and a maximum residual horizontal oscillation of 6 mm for a vertical drop of the scissor lift. The period, T, the time between two successive peaks, of the oscillation was calculated and used to determine the frequency, f, of the system:

$$f = 1/T \tag{2}$$

Figure 26: A scissor lift in the high-bay of the MaRC building at the Georgia Institute of Technology.

Damping ratio, ζ, of the impulse response is calculated using logarithmic decrement:

$$\delta = ln(\frac{x_0}{x_1}) \tag{3}$$

x_0 and x_1 are the amplitudes of two successive peaks of the oscillation.

$$\zeta = \frac{1}{\sqrt{1 + (\frac{2\pi}{\delta})^2}} \tag{4}$$

From the vertical residual oscillation, the frequency and damping ratio of the system were determined to be approximately 4.3 Hz and 0.11, respectively, at this configuration. The same motion was repeated, which resulted in a maximum vertical oscillation of also 10 mm and a maximum horizontal oscillation of 3 mm, as shown in Figure 28. The second experiment's frequency and damping ratio were 4.3 Hz and 0.13, respectively. Th A third trial was conducted, as shown in Figure 29. The vertical drop induced a maximum residual vertical oscillation of 20 mm and a maximum residual horizontal oscillation of 4 mm. The

third vertical drop in the scissor lift indicated a system frequency of only 3.5 Hz and a damping ratio of 0.16. In general, the scissor lift has a frequency range of 3-5 Hz with an average of 4 Hz and an average damping ratio of 0.13.

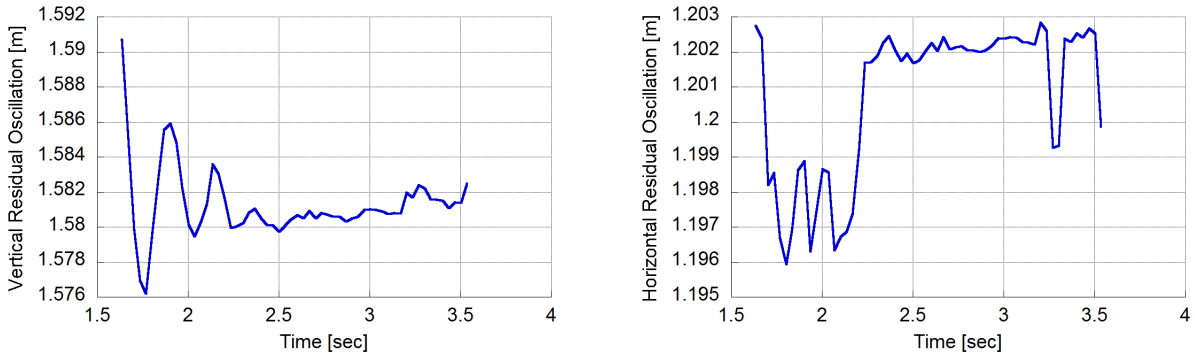

(a) Vertical residual oscillation (b) Horizontal residual oscillation

Figure 27: First residual oscillation recorded from a vertical drop by a scissor lift.

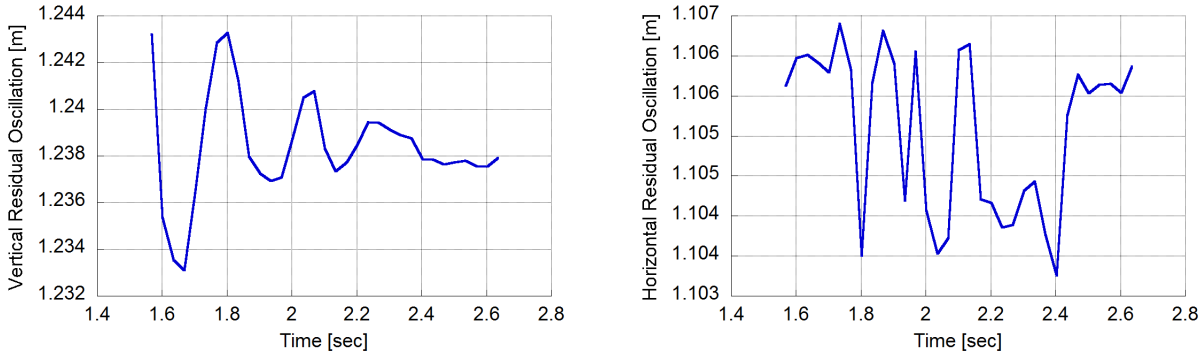

(a) Vertical residual oscillation (b) Horizontal residual oscillation

Figure 28: Second residual oscillation recorded from a vertical drop by a scissor lift.

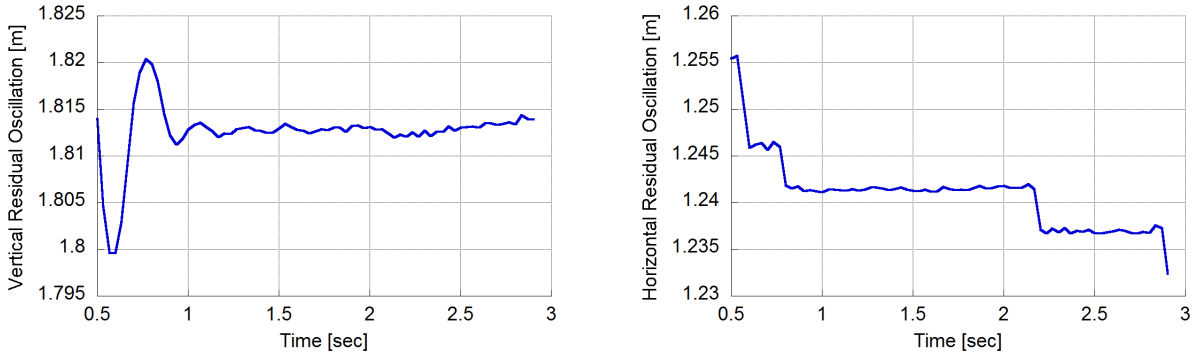

(a) Vertical residual oscillation (b) Horizontal residual oscillation

Figure 29: Third residual oscillation recorded from a vertical drop by a scissor lift.

A larger vertical oscillation amplitude was observed for the third trial compared to the

first and second. A key distinction between trial 3 and trials 1 and 2 is the final position of the lift in trial 3 was much higher than in trials 1 and 2. System frequency depends on the height of the scissor lift platform and the weight on the platform. For these trials, the mass on the platform did not change; however, the height of the platform did change from trials 1 and 2 to trial 3. In general, the oscillation in the vertical direction was always larger than in the horizontal direction. The average vertical oscillation was 13.33 mm and the average horizontal oscillation was 4.33 mm. The results of these experiments are summarized in Table 4.

Table 4: Residual oscillation from vertical drops of a scissor lift in millimeters.

	Trial 1	**Trial 2**	**Trial 3**	**Average**
Maximum Vertical Oscillation [mm]	10	10	20	13.33
Maximum Horizontal Oscillation [mm]	6	3	4	4.33
Frequency [Hz]	4.3	4.3	3.5	4.03
Damping Ratio	0.11	0.13	0.16	0.13

2.1.2 Operator-Induced oscillations

Oscillations of a scissor lift can also be caused by the operator applying forces to the elevated platform. If the operator reaches over the sides of the scissor lift and tries to grab or pull something, it will move the lift and induce deflection and oscillation. To demonstrate these types of residual oscillation, the scissor lift shown in Figure 26 was raised to a height of 5.09 meters and the operator on the platform holding onto the rails leaned quickly to one side of the platform across the shorter length, as shown in Figure 30 by the dashed blue arrowed line. In the figure, the front of the platform is green and the front of the base is gray.

The quick lean and resulting residual oscillation were recorded with a video camera. Using Matlab, the video was analyzed to quantify the amount of residual oscillation caused by the motion of the scissor lift. Figure 31 shows a maximum horizontal residual oscillation of 51 mm from the first experiment. A second trial showed a maximum horizontal residual oscillation of 40 mm, as shown in Figure 32. The first trial had a frequency of 1.2 Hz, damping ratio of 0.12, and the second trial had a frequency of 0.9 Hz, damping ratio of

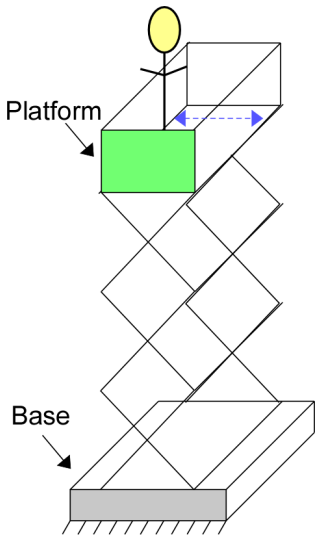

Figure 30: Diagram of impulse conducted on scissor lift.

0.16.

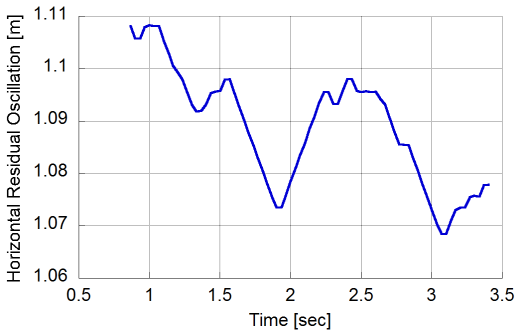

Figure 31: Horizontal residual oscillation of side to side impulse on a scissor lift.

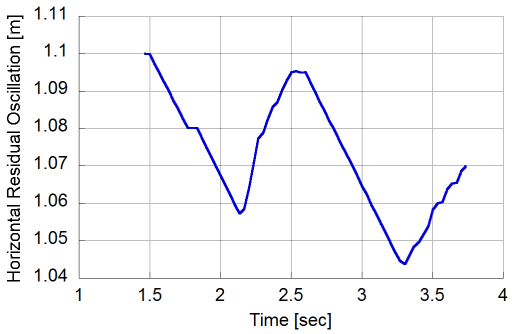

Figure 32: Second horizontal residual oscillation of side to side impulse on a scissor lift.

2.2 Aerial Lift Machine-Motion Induced oscillation

Figure 33, shows another type of aerial lift called a cherry picker. While the operators in the work platform repositioned the aerial lift, a video was taken to analyze the machine response. An average male height was used as a calibrating factor on the person on the platform to determine distances in the video. A vertical residual oscillation of 0.358 m and a horizontal residual oscillation of 0.227 m were observed, as shown in Figure 34. From these results, the system's frequency was 1.5 Hz with a range from 1 - 2 Hz and the damping ratio was 0.1. In comparison to the scissor lift, the aerial lift has more oscillation and

approximately the same frequency as the scissor lift under side-to-side displacements.

(a) Back-side view of aerial lift

(b) Front-side view of aerial lift

Figure 33: Aerial lifts seen working together near Georgia Tech.

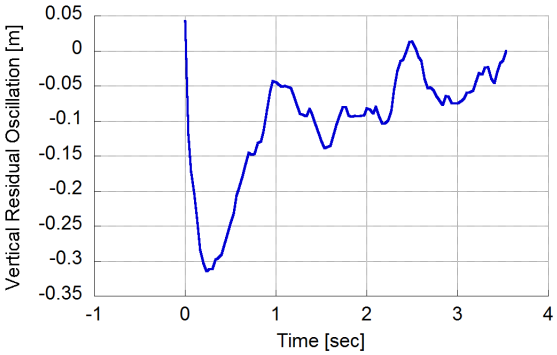

(a) Vertical residual oscillation

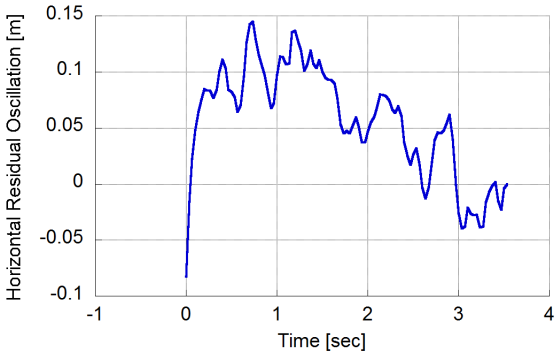

(b) Horizontal residual oscillation

Figure 34: Residual oscillation from an observed aerial lift movement.

2.3 Summary

From all these experiments of the different aerial lifts, scissor lift and articulating aerial lift, a clear observation is that oscillations result from the movement of the aerial lift or the operator working in the elevated platform. From the oscillations observed there is a risk of obstacle collision; thus, oscillation control is important. From the experiments, articulating aerial lift result in larger oscillations due to movement than a scissor lift. Therefore, in the following chapters, further study of oscillation is conducted on a small-size cherry picker with similar oscillation frequency and damping ratio as the articulating aerial lift analyzed in this chapter.

CHAPTER III

DYNAMIC OSCILLATION ANALYSIS OF DOUBLE-BOOM ARTICULATING AERIAL LIFT

From previous research, it is known that movements of telescopic aerial lifts induce large and dangerous oscillations in luffing and slewing motions [20]. Articulating aerial lifts have greater residual oscillation when the booms are in an extended configuration compared to a compact configuration [10]. There is also greater oscillation when the platform is carrying more weight [17]. In addition, residual oscillation by luffing moves for non-overcenter articulating aerial lifts were investigated and reduced through input shaping [10]. Residual oscillation from slewing moves and by overcenter articulating aerial lifts are to be investigated in this chapter.

3.1 Model Description

The model shown in Figure 35 was used to analyze the oscillation of a double-boom articulating aerial lift. The aerial lift is composed of five bodies: base, rotating tower, lower boom, upper boom, and payload. The base, the bottom of the aerial lift, has dimensions listed in Table 5 and shown in Figure 36. Figure 37 shows the rotating tower is located a distance away from the center of the base, to the backside of the aerial lift's base. Its properties are listed in Table 6. Mounted to the top of the rotating tower are the double booms and payload of the aerial lift with set lengths from L_1 to L_3. Their properties are also listed in Table 6.

The booms slew from the rotating tower an angle of θ_1 with respect to the fixed base, as shown in Figure 36. The lower boom luffs from the base by θ_2 and the upper boom luffs from the lower boom by θ_3. The connection between the rotating tower and the lower boom is known as the shoulder joint; thus, θ_2 is known as the shoulder angle. The connection between the lower boom and the upper boon is know as the elbow joint; thus, θ_3 is known

Table 5: Base parameters and measurements.

Parameters	Value	Units	Variable
Base mass	4.2	kg	M_T
Base length	1.04	m	TL
Base width	0.5	m	TW
Distance to rotating tower	0.05	m	LC

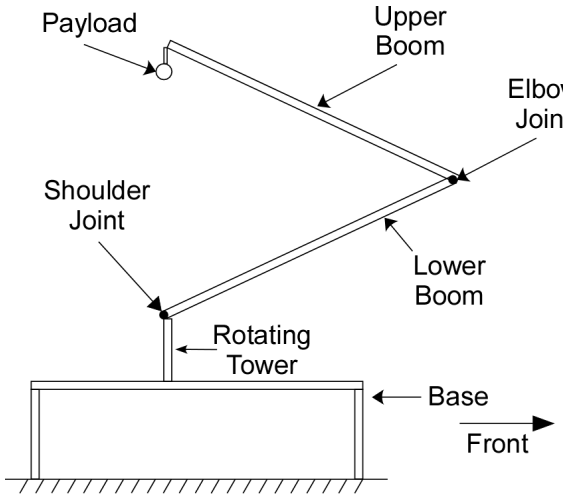

Figure 35: Double-boom articulating aerial lift.

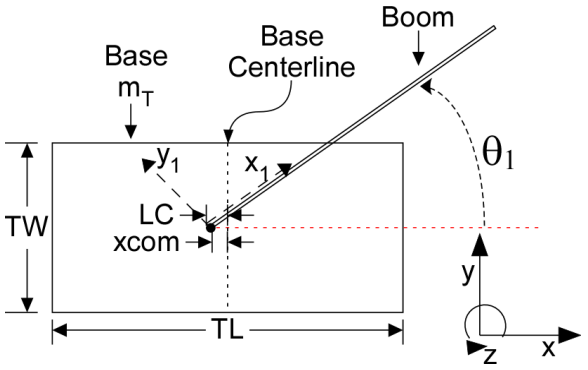

Figure 36: Top view of dynamic model articulating aerial lift.

Table 6: Lengths and masses of model articulating lift.

Part	Length [m]	Variable	Mass [kg]	Variable
Rotating Tower	0.195	L_0	1	M_0
Lower Boom	1	L_1	2	M_1
Upper Boom	1	L_2	2	M_2
Payload	0.05	L_3	2	M_3

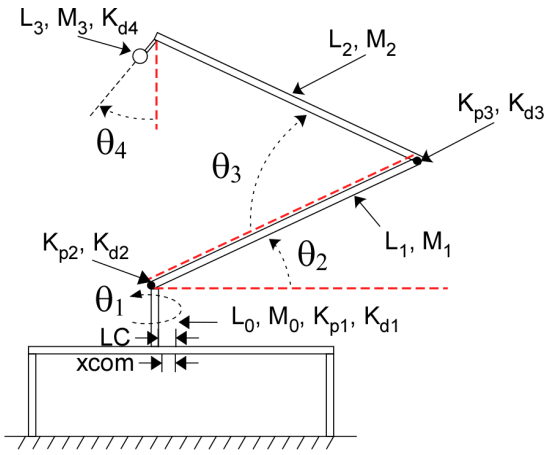

Figure 37: Dynamic model of double-boom articulating aerial lift.

as the elbow angle. Lastly, the payload swings through angle θ_4, side-to-side in response to the flexibility of the system. To model flexibility of the system, lumped rotational spring-dampers were used at the joints between booms that luff and about the rotating tower's vertical axis for the slewing motion. Other research has used the elastic properties of the aerial lift material to demonstrate such flexibility [6, 7]. Table 7 shows the spring, K_p, and damper, K_d, constants used that came from previous research [10]. These constants create similar frequency and damping ratio as a life-size cherry picker. The payload is modeled as a free swinging damped pendulum. Its oscillation flexibility arises from gravity as the spring force. The x coordinate of the base's center of mass is located at distance $xcom$ from the center of the base, as shown in Figure 36. Both of the y and z coordinate of the base's center of mass are located a distance of zero from the center of the base.

Table 7: Flexibility parameters.

Joint	K_p **[N/m]**	K_d **[N sec/m]**
Rotating Tower	500	20
Shoulder	3500	40
Elbow	2000	40
Payload	-	1

Other researchers have investigated a related machine that is a fire-rescue turntable ladder. The turning and raising velocities in that research were set to $4.5°/sec$ and $3°/sec$, respectively [21]. For this model of an articulating aerial lift the velocities were set to

$10°/sec$ because the booms of the aerial lift do not have people climbing on them while in motion and because their booms are more of an enclosed structure compared to a fire-rescue turntable ladder. The accelerations were set to $40°/sec^2$, as shown in Table 8. All moves by the model aerial lift were given trapezoidal velocity profiles to follow. In addition, oscillations of the booms and payload were analyzed at the end of the velocity profile. This is called the residual oscillation from a move.

Table 8: Velocity and acceleration limits.

	Limit
Velocity	$10°$/sec
Acceleration	$40°/sec^2$

The x, y, and z reference frame is fixed to the base of the aerial lift. z is along the rotating tower and the positive z direction is up. x is parallel to the base's lengthwise edge and the positive x direction is toward the front of the aerial lift, as denoted in Figure 35. y is parallel to the base's widthwise edge and the positive y direction is into the page of Figure 35. Figure 36 shows that θ_1 slews around the aerial lift's vertical axis, the z-axis. For a slew of θ_1 the x and y axes are rotated to the new x_1 and y_1 axes, as shown in Figure 36. θ_2 and θ_3 luff initially around the aerial lift's horizontal axis, the y-axis. Most articulating aerial lifts begin in a compact configuration with the upper boom laying on top of or next to the lower boom; thus, the booms luff in opposite directions. θ_2 luffs in a counter-clockwise direction; thus, the rotation matrix for $-\theta_2$ in the y direction is used. The rotation matrices $R_z(\theta_1)$ (5), $R_y(-\theta_2)$ (6)and $R_y(\theta_3)$ (7) for this model are:

$$\mathbf{R_z}(\theta_\mathbf{1}) = \begin{bmatrix} cos\theta_1 & -sin\theta_1 & 0 \\ sin\theta_1 & cos\theta_1 & 0 \\ 0 & 0 & 1 \end{bmatrix} \tag{5}$$

$$\mathbf{R_y}(-\theta_\mathbf{2}) = \begin{bmatrix} cos\theta_2 & 0 & -sin\theta_2 \\ 0 & 1 & 0 \\ sin\theta_2 & 0 & cos\theta 2 \end{bmatrix} \tag{6}$$

$$\mathbf{R_y}(\theta_3) = \begin{bmatrix} cos\theta_3 & 0 & sin\theta_3 \\ 0 & 1 & 0 \\ -sin\theta_3 & 0 & cos\theta_3 \end{bmatrix} \tag{7}$$

To have x, y, and z coordinates in the Newtonian frame, multiply the rotation matrices:

$$\begin{bmatrix} x \\ y \\ z \end{bmatrix} = R_z(\theta_1)R_y(-\theta_2)R_y(\theta_3) \begin{bmatrix} x_3 \\ y_3 \\ z_3 \end{bmatrix} \tag{8}$$

The following equations were used to determine the transient position of the end-effector and the steady-state position of the end-effector in the x, y, or z directions. The lengths of the booms of the model were 1 meter to simplify the following equations. To determine residual oscillation of the booms and rotating tower the steady-state position was subtracted from the transient position of the end-effector:

$$x = cos(\theta_1)(-cos(\theta_3 - \theta_2) + cos(\theta_2)) \tag{9}$$

$$y = sin(\theta_1)(-cos(\theta_3 - \theta_2) + cos(\theta_2)) \tag{10}$$

$$z = sin(\theta_3 - \theta_2) + sin(\theta_2) \tag{11}$$

The overall oscillation amplitude is given by:

$$Oscillation \;\; Amplitude = \sqrt{x^2 + y^2 + z^2} \tag{12}$$

x, y, and z are the residual oscillation in those directions calculated by equations (9)-(11). Using a commercially available dynamics software [14], the model double-boom articulating aerial lift's four equations of motion for the four generalized coordinates, θ_1, θ_2, θ_3, and θ_4, were obtained:

$$K_{p1}(\theta_{1d} - \theta 1) + K_{d1}(\dot{\theta}_{1d} - \dot{\theta}_1) + ({}^2/_3)\dot{\theta}_1(M_1 L_1^2 \sin(\theta_2)\cos(\theta_2)\dot{\theta}_2$$
$$- M_2(1.5L_1 L_2 \sin(\theta_2)\cos(\theta_2 - \theta_3)\dot{\theta}_2 + 1.5L_1 L_2 \cos(\theta_2)\sin(\theta_2 - \theta_3)(\dot{\theta}_2 - \dot{\theta}_3)$$
$$- 3L_1^2 \sin(\theta_2)\cos(\theta_2)\dot{\theta}_2 - L_2^2 \sin(\theta_2 - \theta_3)\cos(\theta_2 - \theta_3)(\dot{\theta}_2 - \dot{\theta}_3)) - 3M_3(L_1 L_3 \sin(\theta_2)$$
$$\sin(\theta_4)\dot{\theta}_2 + L_3^2 \sin(\theta_4)\cos(\theta_4)\dot{\theta}_4 + L_1 L_2 \sin(\theta_2)\cos(\theta_2 - \theta_3)\dot{\theta}_2 + L_2 L_3 \cos(\theta_4)$$
$$\cos(\theta_2 - \theta_3)\dot{\theta}_4 + L_1 L_2 \cos(\theta_2)\sin(\theta_2 - \theta_3)(\dot{\theta}_2 - \dot{\theta}_3) - L_1 L_3 \cos(\theta_2)\cos(\theta_4)\dot{\theta}_4$$
$$- L_1^2 \sin(\theta_2)\cos(\theta_2)\dot{\theta}_2 - L_2 L_3 \sin(\theta_4)\sin(\theta_2 - \theta_3)(\dot{\theta}_2 - \dot{\theta}_3) - L_2^2 \sin(\theta_2 - \theta_3)\cos(\theta_2 - \theta_3)$$
$$(\dot{\theta}_2 - \dot{\theta}_3))) - ({}^1/_3)(1.5M_0 r_c^2 + M_1 L_1^2 \cos(\theta_2)^2 + M_2 L_2^2 \cos(\theta_2 - \theta_3)^2 + 3L_1 M_2 \cos(\theta_2)$$
$$(L_1 \cos(\theta_2) - L_2 \cos(\theta_2 - \theta_3)) - 3M_3(2L_1 L_3 \sin(\theta_4)\cos(\theta_2) + 2L_1 L_2 \cos(\theta_2)\cos(\theta_2 - \theta_3) - L_1^2$$
$$\cos(\theta_2)^2 - L_3^2 \sin(\theta_4)^2 - L_2^2 \cos(\theta_2 - \theta_3)^2 - 2L_2 L_3 \sin(\theta_4)\cos(\theta_2 - \theta_3)))\ddot{\theta}_1 = 0 \tag{13}$$

$$K_{p2}(\theta_{2d} - \theta_2) + K_{d2}(\dot{\theta}_{2d} - \dot{\theta}_2) - 0.5gL_1 M_1 \cos(\theta_2) - gM_3(L_1 \cos(\theta_2) - L_2 \cos(\theta_2 - \theta_3))$$
$$- 0.5gM_2(2L_1 \cos(\theta_2) - L_2 \cos(\theta_2 - \theta_3)) - ({}^1/_3)M_1 L_1^2 \sin(\theta_2)\cos(\theta_2)\dot{\theta}_1^2$$
$$- ({}^1/_3)M_2 L_2^2 \sin(\theta_2 - \theta_3)\cos(\theta_2 - \theta_3)\dot{\theta}_1^2 - 0.5L_1 M_2(2L_1 \sin(\theta_2)\cos(\theta_2)\dot{\theta}_1^2$$
$$+ L_2 \sin(\theta_3)(\dot{\theta}_2^2 + \cos(\theta_2)^2\dot{\theta}_1^2) - L_2 \sin(\theta_2)\cos(\theta_2)\cos(\theta_3)\dot{\theta}_1^2 - L_2 \cos(\theta_3)\sin(\theta_2 - \theta_3)$$
$$\cos(\theta_2 - \theta_3)\dot{\theta}_1^2 - L_2 \sin(\theta_3)((\dot{\theta}_2 - \dot{\theta}_3)^2 + \cos(\theta_2 - \theta_3)^2\dot{\theta}_1^2)) - M_3(L_1 L_3 \cos(\theta_2 + \theta_4)\dot{\theta}_4^2$$
$$+ L_1^2 \sin(\theta_2)\cos(\theta_2)\dot{\theta}_1^2 + L_1 L_2 \sin(\theta_3)(\dot{\theta}_2^2 + \cos(\theta_2)^2\dot{\theta}_1^2) + L_2 \sin(\theta_2 - \theta_3)(L_3 \sin(\theta_4)$$
$$+ L_2 \cos(\theta_2 - \theta_3))\dot{\theta}_1^2 - L_2 L_3 \cos(\theta_3 - \theta_2 - \theta_4)\dot{\theta}_4^2 - L_1 L_2 \sin(\theta_2)\cos(\theta_2)\cos(\theta_3)\dot{\theta}_1^2$$
$$- L_1 \cos(\theta_3)\sin(\theta_2 - \theta_3)(L_3 \sin(\theta_4) + L_2 \cos(\theta_2 - \theta_3))\dot{\theta}_1^2 - L_1 \sin(\theta_3)$$
$$(L_3 \sin(\theta_4)\cos(\theta_2 - \theta_3)\dot{\theta}_1^2 + L_2((\dot{\theta}_2 - \dot{\theta}_3)^2 + \cos(\theta_2 - \theta_3)^2\dot{\theta}_1^2))) - L_3 M_3(L_1 \sin(\theta_2 + \theta_4)$$
$$+ L_2 \sin(\theta_3 - \theta_2 - \theta_4))\ddot{\theta}_4 - ({}^1/_3)L_2(1.5L_1 M_2 \cos(\theta_3) - L_2 M_2 - 3M_3(L_2 - L_1 \cos(\theta_3)))\ddot{\theta}_3$$
$$- ({}^1/_3)(M_1 L_1^2 + M_2 L_2^2 + 3L_1 M_2(L_1 - L_2 \cos(\theta_3)) + 3M_3(L_1^2 + L_2^2 - 2L_1 L_2 \cos(\theta_3)))\ddot{\theta}_2 = 0 \tag{14}$$

$$K_{p3}(\theta_{3d}-\theta_3)+K_{d3}(\dot{\theta}_{3d}-\dot{\theta}_3)+L_2L_3M_3\sin(\theta_3-\theta_2-\theta_4)\ddot{\theta}_4-gL_2M_3\cos(\theta_2-\theta_3)$$
$$-0.5gL_2M_2\cos(\theta_2-\theta_3)-(^1/_3)L_2(M_2(1.5L_1\sin(\theta_2)\cos(\theta_2)\cos(\theta_3)\dot{\theta}_1^2$$
$$-1.5L_1\sin(\theta_3)(\dot{\theta}_2^2+\cos(\theta_2)^2\dot{\theta}_1^2)-L_2\sin(\theta_2-\theta_3)\cos(\theta_2-\theta_3)\dot{\theta}_1^2)+3M_3(L_3\cos(\theta_3-\theta_2-\theta_4)\dot{\theta}_4^2$$
$$+L_1\sin(\theta_2)\cos(\theta_2)\cos(\theta_3)\dot{\theta}_1^2-L_3\sin(\theta_4)\sin(\theta_2-\theta_3)\dot{\theta}_1^2-L_1\sin(\theta_3)(\dot{\theta}_2^2+\cos(\theta_2)^2\dot{\theta}_1^2)$$
$$-L_2\sin(\theta_2-\theta_3)\cos(\theta_2-\theta_3)\dot{\theta}_1^2))-(^1/_3)L_2^2(M_2+3M_3)\ddot{\theta}_3$$
$$-(^1/_3)L_2(1.5L_1M_2\cos(\theta_3)-L_2M_2-3M_3(L_2-L_1\cos(\theta_3)))\ddot{\theta}_2=0 \tag{15}$$

$$L_2L_3M_3\sin(\theta_3-\theta_2-\theta_4)\ddot{\theta}_3-gL_3M_3\sin(\theta_4)-K_{d4}\dot{\theta}_4-L_3M_3(L_1\sin(\theta_2)\cos(\theta_2)$$
$$\sin(\theta_2+\theta_4)\dot{\theta}_1^2+L_1\cos(\theta_2+\theta_4)(\dot{\theta}_2^2+\cos(\theta_2)^2\dot{\theta}_1^2)+\sin(\theta_2-\theta_3)\sin(\theta_3-\theta_2-\theta_4)(L_3\sin(\theta_4)$$
$$+L_2\cos(\theta_2-\theta_3))\dot{\theta}_1^2-\cos(\theta_3-\theta_2-\theta_4)(L_3\sin(\theta_4)\cos(\theta_2-\theta_3)\dot{\theta}_1^2+L_2((\dot{\theta}_2-\dot{\theta}_3)^2$$
$$+\cos(\theta_2-\theta_3)^2\dot{\theta}_1^2)))-M_3L_3^2\ddot{\theta}_4-L_3M_3(L_1\sin(\theta_2+\theta_4)+L_2\sin(\theta_3-\theta_2-\theta_4))\ddot{\theta}_2=0 \tag{16}$$

In the equations of motion, rc is the radius of the rotating tower, 0.025 m, and the angles with d subscripts represent desired position or velocity. The parameters in Tables 5-8 were used to simulate the dynamic characteristics of the double-boom articulating lift.

3.2 Overcenter Luffing Effects

Luffing moves for non-overcenter articulating aerial lifts were investigated and reduced through input shaping [10]. The effects of a shoulder moves at different initial elbow angles showed that as the elbow angle changes the booms of the aerial lift into an increasingly extended configuration, the residual amplitude increases. However, the previous research did not include overcenter configurations for the initial elbow angles. By allowing the elbow angle to pass 180° and again executing a shoulder move, the residual amplitude decreases at overcenter configurations. In Figure 38 the initial shoulder angle was 30°, the shoulder move was 60°, and the initial elbow angles ranged from 0° to 240° in increments of 4° to show the effect of decreased oscillation in overcenter configurations. The greatest maximum residual amplitude was 8.7 mm and occurred at an initial elbow angle of 180°.

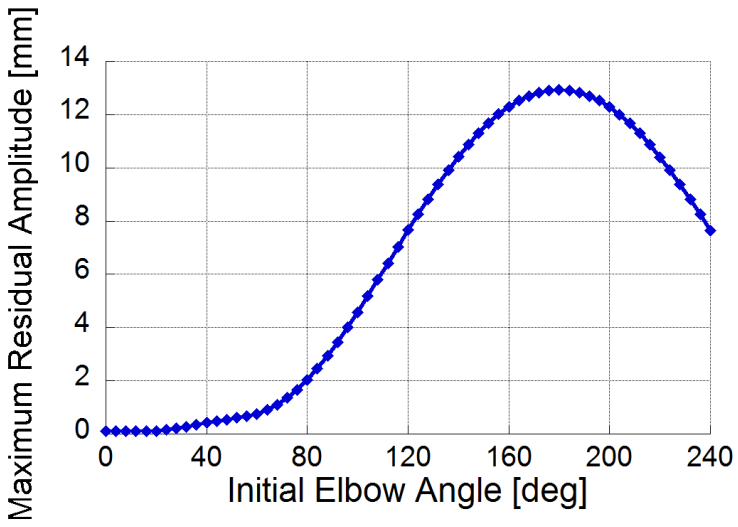

Figure 38: Residual amplitude from a shoulder move from 30° to 90° with different initial elbow angles.

Figure 39 shows the largest maximum residual amplitude configuration and move.

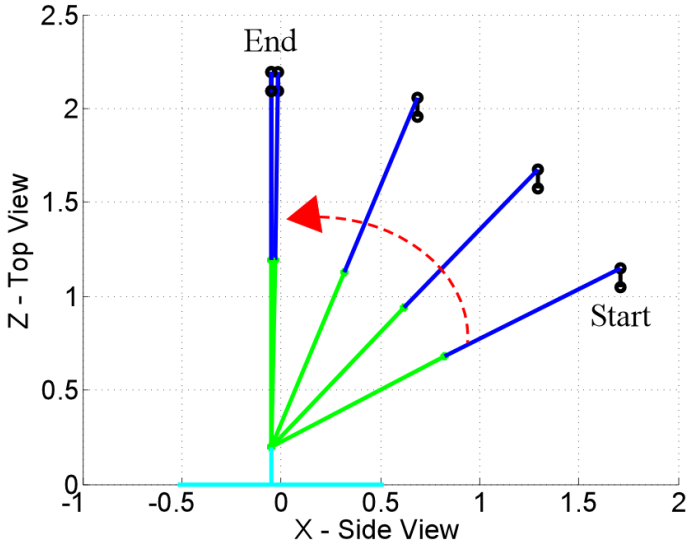

Figure 39: Residual amplitude from a shoulder move from 30° to 90° with initial elbow angle 180°.

When the initial elbow angle is 0° the cherry picker is in configuration 1 as shown in Figure 40. Configuration 2 is at the largest maximum residual amplitude and configuration 3 is the final overcenter configuration with the elbow angle as 240°.

To investigate the effect of the initial shoulder angle on the residual amplitude, initial shoulder angles were also varied from 0° to 120° in increments of 10° with the varied initial

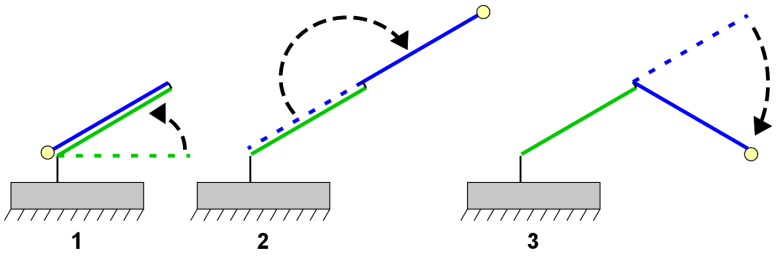

Figure 40: Significant configurations of cherry picker during a 60° shoulder move with different initial elbow angles.

elbow angles. Figure 41 shows a trend of decreasing residual amplitude after overcenter for different initial shoulder angles. The shoulder move for Figure 41 was 60°. The largest residual amplitude was 12.37 mm and occurred at an initial shoulder and elbow angles of 50° and 180°, respectively, as shown in Figure 42.

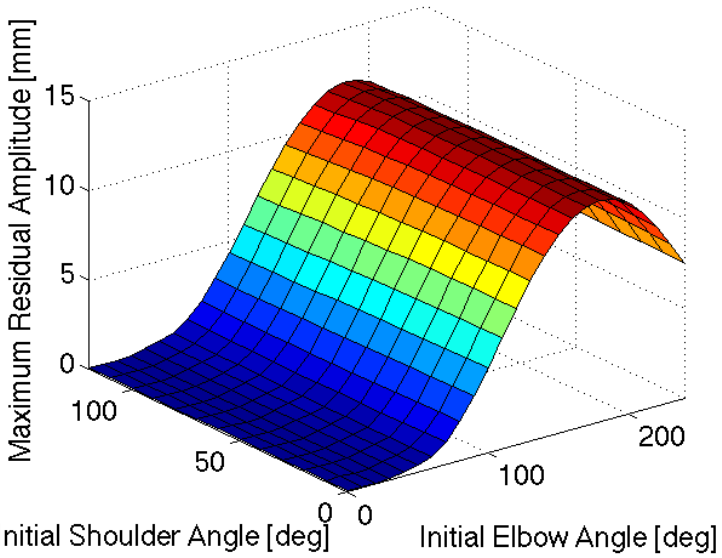

Figure 41: Residual amplitude resulting from a 60° shoulder move with different initial elbow and shoulder angles.

Oscillation decreases when the cherry picker is in a more compact overcenter configuration because of the aerial lift's moment arm in that configuration is shorter than the moment arm in the extended non-overcenter configuration before entering the overcenter configuration.

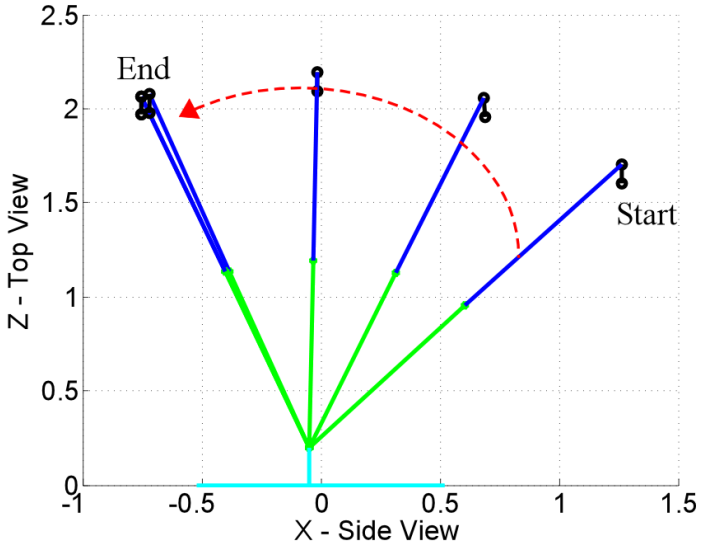

Figure 42: Largest maximum residual amplitude resulting from a 60° shoulder move with initial shoulder and elbow angles of 50° and 180°, respectively.

3.3 Slewing Effects

3.3.1 Slewing Only Oscillation

Besides luffing a cherry picker is able to slew. To investigate the effects of slewing the small-scale cherry picker was slewed 160° in an extended configuration of the shoulder angle at 30° and the elbow angle at 160°, as shown in Figure 43.

Figure 44 shows the oscillatory response of the tip of the boom in the x direction and the y direction at the completion of the slew. Little oscillation occurred in the z direction because slewing does not change the booms' vertical position. The booms oscillated with a frequency of approximately 1.21 Hz and a damping ratio of 0.155. The same frequency and damping ratio equations as in Chapter 2 were used. Maximum displacement of the tip of the arm was 4.8 mm in the x direction and 13.06 mm in the y direction.

Extended configurations result in large residual oscillations. Figure 45 shows the residual oscillation in the x and y directions for a slew move on a compact cherry picker. For the compact cherry picker slew move simulation, the initial shoulder angle was set to 30°, initial elbow angle was set to 90°, and the slewing move was 160°. The compact cherry picker's maximum residual oscillation in the x direction was 0.1 mm and 0.3 mm in the y direction.

Keeping initial elbow angles as in Section 3.2 and performing a slew move instead of a

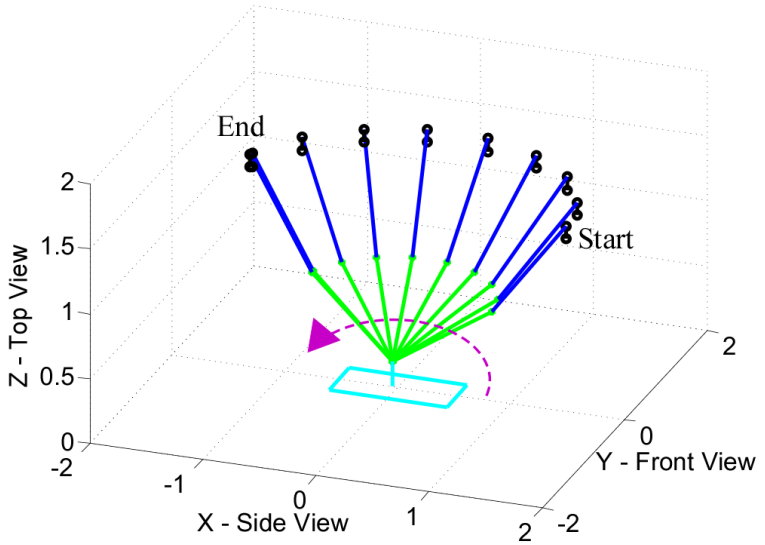

Figure 43: Cherry picker configuration of 30° shoulder angle and 160° elbow angle with a displacement of slew of 160°.

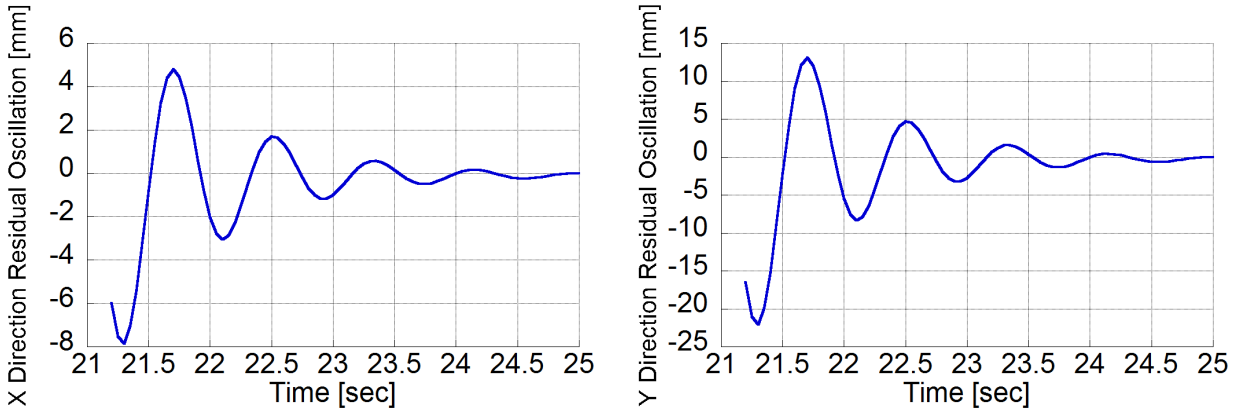

(a) X Direction residual oscillation (b) Y Direction residual oscillation

Figure 44: Residual oscillation from a 160° slew move of a cherry picker in an extended configuration.

shoulder luff move, similar overcenter effects are seen. As the initial elbow angle increases, the booms of the cherry picker extend outward. This results in a longer moment arm and increased oscillation. However, the oscillation stops increasing when the boom reaches an overcenter position, as shown in Figure 46 where the slewing move was 60° and the initial shoulder angle was set to 30°.

The largest residual amplitude was 35.38 mm and occurred at an initial elbow angle of 210°, the equivalent horizontal angle for a shoulder angle 30°, as shown in Figure 47.

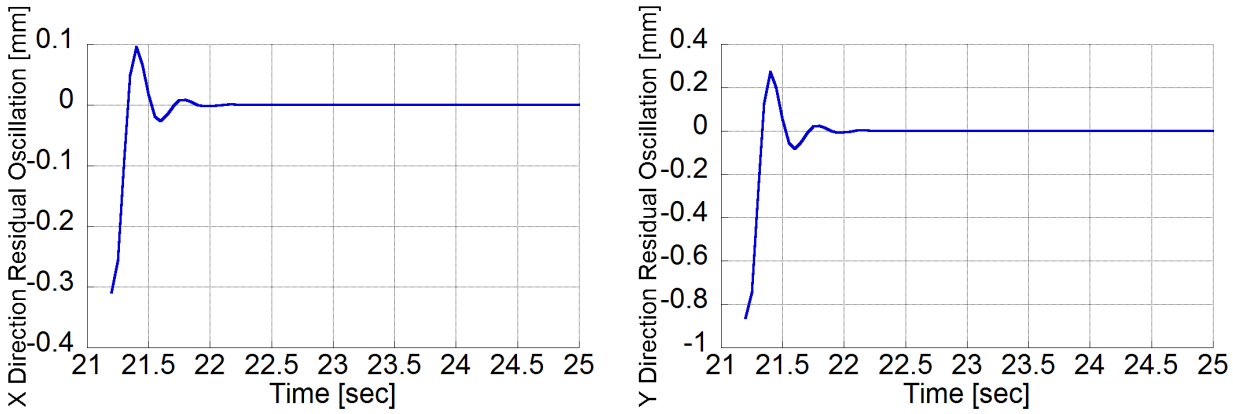

(a) X Direction residual oscillation (b) Y Direction residual oscillation

Figure 45: Residual oscillation from a 160° slew move of a cherry picker in a compact configuration.

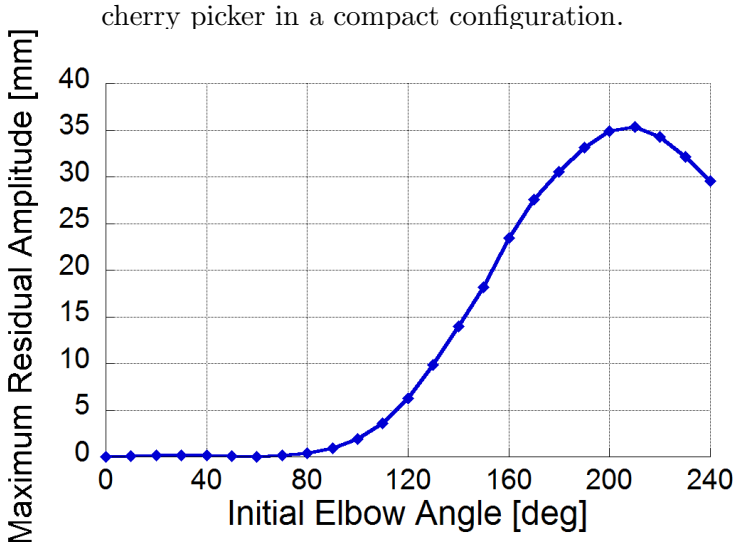

Figure 46: Residual amplitude from a 60° slew move with different initial elbow angles.

Equivalent horizontal angle is the angle that makes the body horizontal. For example, if the lower boom was at an angle of 30°, then the upper boom's equivalent horizontal angle is 210° because subtracting 30° from 210° gives 180° which would be the horizontal angle if the lower boom was at an angle of 0°. Equivalent horizontal angles are the angle at which the longest moment arm would occur because that is when the cherry picker is reaching the farthest away from the center of the support base.

When the initial elbow angle is 0° the cherry picker is in configuration 1 as shown in Figure 48. Configuration 2 is at the largest maximum residual amplitude and configuration 3 is the final overcenter configuration with the elbow angle as 240°.

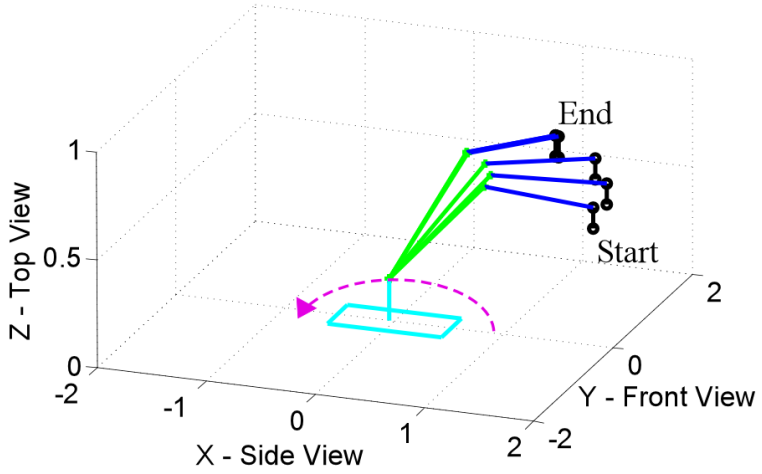

Figure 47: Largest residual amplitude from a 60° slew move occurred at an initial elbow angle of 210°.

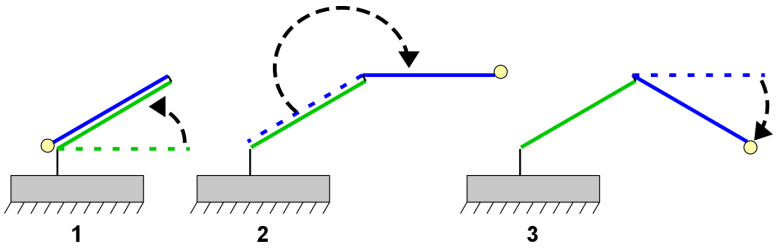

Figure 48: Significant configurations of cherry picker during a 60° slew move with different initial elbow angles.

To investigate the effect of the initial shoulder angle on residual amplitude, Figure 49 shows initial elbow and shoulder angles varied for a slew move of 60°. The initial shoulder angles expand into overcenter locations for the lower boom as they are varied from 0° to 120° in increments of 10°. At overcenter configurations for the lower boom the aerial lift begins slewing from the opposite side of the base toward the slew angle of 270° similar to slewing from 0° toward 90°. With the upper boom extended horizontal on either side the residual amplitude increases; thus, there are residual amplitude peaks on both ends of the figure. However, the initial shoulder angles were only varied to 120° prohibiting the second peak along the y-axis from reaching the equivalent magnitude of the x-axis peak. Again by changing to overcenter upper boom configurations the residual amplitude decreases again because the booms are brought closer to the center of the aerial lift decreasing the moment arm.

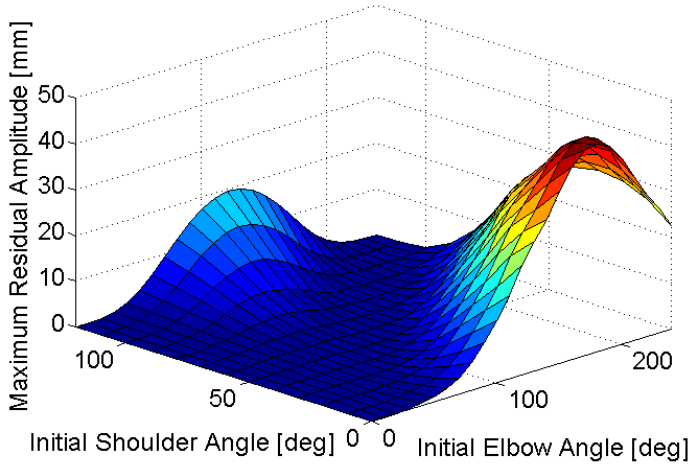

Figure 49: Residual amplitude resulting from a 60° slew move with different initial elbow and shoulder angles.

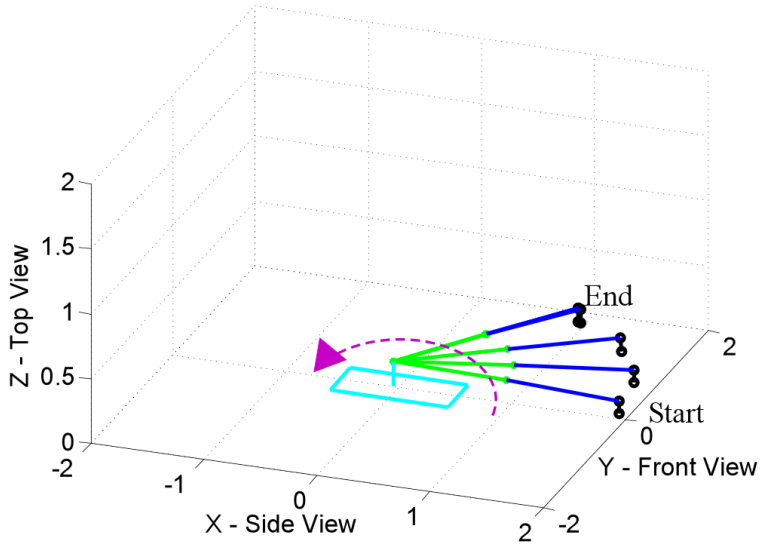

Figure 50: Largest residual amplitude from a 60° slew move occurred at an initial shoulder and elbow angles of 0° and 180°, respectively.

The largest residual amplitude was 45.51 mm and occurred at initial shoulder and elbow angles of 0° and 180°, respectively, as shown in Figure 50.

The second peak in residual amplitude occurred at an initial shoulder and elbow angles of 120° and 120°, respectively, as shown in Figure 51. The 120° elbow angle is the equivalent horizontal angle for a shoulder angle of 120°.

To generalize the effect of slewing moves for a compact cherry picker, the cherry picker's

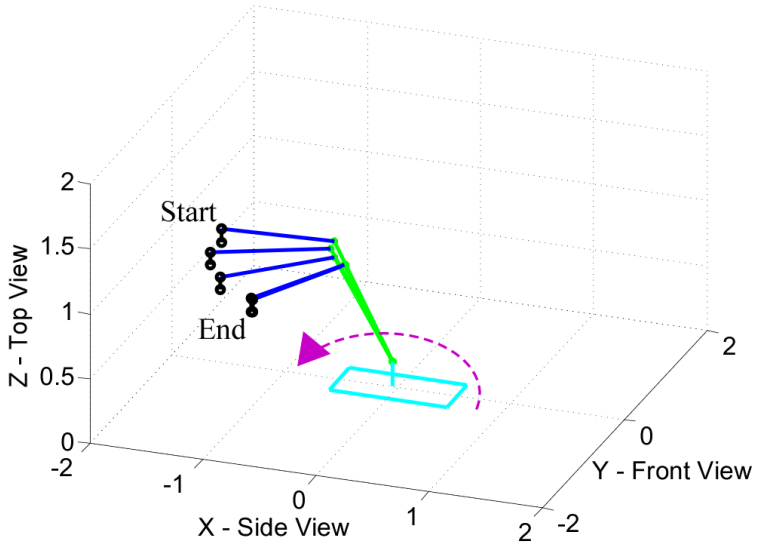

Figure 51: Second peak in residual amplitude from a 60° slew move occurred at an initial shoulder and elbow angles of 120° and 120°, respectively.

initial shoulder angle was set to 30° and the initial elbow angle was set to 90°, a semi-compact configuration. Figure 52(a) shows that residual amplitude from performing varied slewing moves from 0° to 300° in increments of 5° on the compact configuration plateaus after a certain slew move. For a compact cherry picker residual amplitude plateaus at approximately 10° slew move. Performing the same slew moves on an extended cherry picker with an initial shoulder angle of 30°, an initial elbow angle of 160° shows that residual amplitude also plateaus after a certain slew move except it first peaks at a higher residual amplitude than it plateaus. For the extended configuration the residual amplitude plateaus at approximately 30°, as shown in Figure 52(b). The extended cherry picker reached a maximum of 35.19 mm residual amplitude and later plateaued at approximately 23 mm. The compact cherry picker plateaued at a residual amplitude of approximately 0.92 mm. Some two-mode oscillations can also be seen from this extended configuration.

Figure 53 shows the configurations for the compact and extended cherry pickers used to show the generalized slewing effects.

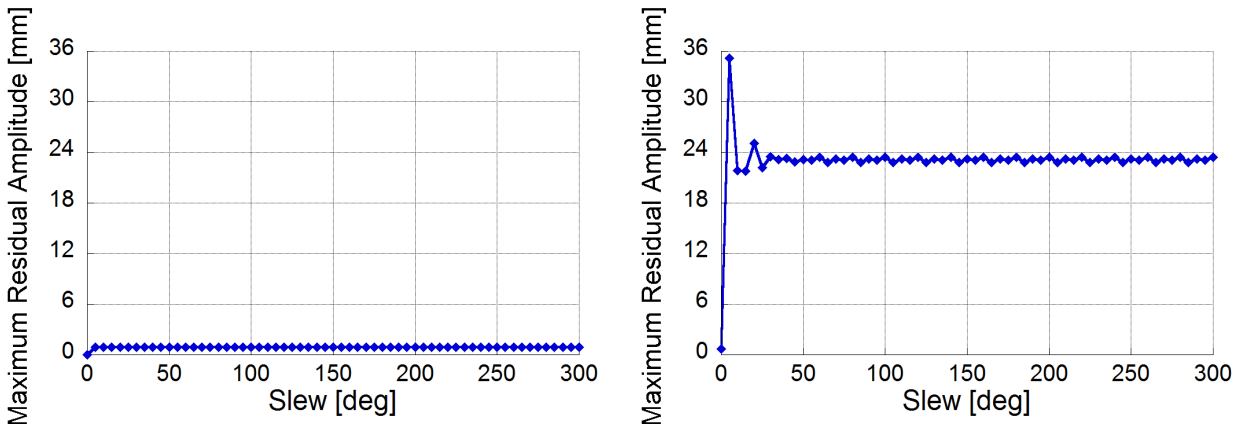

(a) Compact cherry picker (b) Extended cherry picker

Figure 52: Residual amplitude of slew moves from 0° to 300° of a cherry picker.

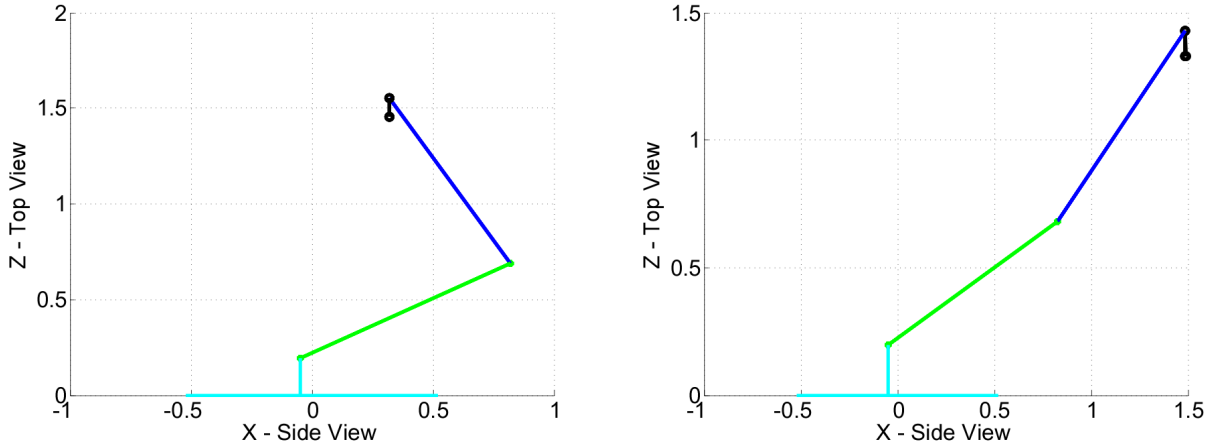

(a) Compact cherry picker (b) Extended cherry picker

Figure 53: Configurations of compact and extended cherry pickers for slew moves.

Figure 54 shows the maximum residual oscillation in x, y, and z directions for different slew displacements from 0° to 300° in increments of 5° for an initial elbow angle of 120°. Residual oscillations in the x and y directions contribute more to the overall residual amplitude than the z direction residual oscillations.

Maximum residual oscillation in x and y directions for initial elbow angles of 60°, 120°, 180°, and 240° across different slew displacements from 0° to 300° in increments of 5°, as shown in Figure 55, shows how increasing the initial elbow angle increases the maximum residual oscillation because the cherry picker is changing into extended configurations with longer moment arms. The effects of two-mode oscillation for extended configurations is also visible at initial elbow angles of 180° and 240°.

Figure 56 shows the maximum residual oscillation in the x, y, and z directions for

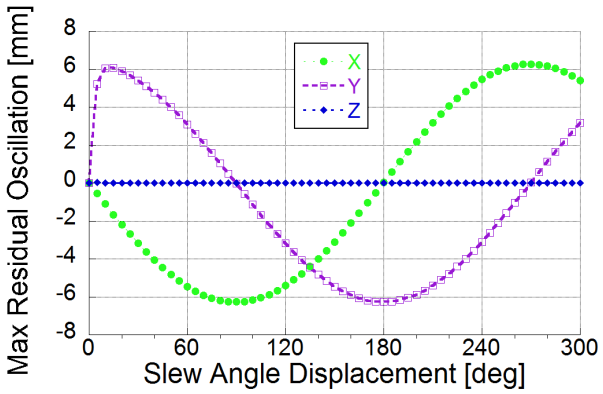

Figure 54: Comparison of maximum residual oscillations in the x, y, and z directions for different slew moves at a set elbow angle of 120°.

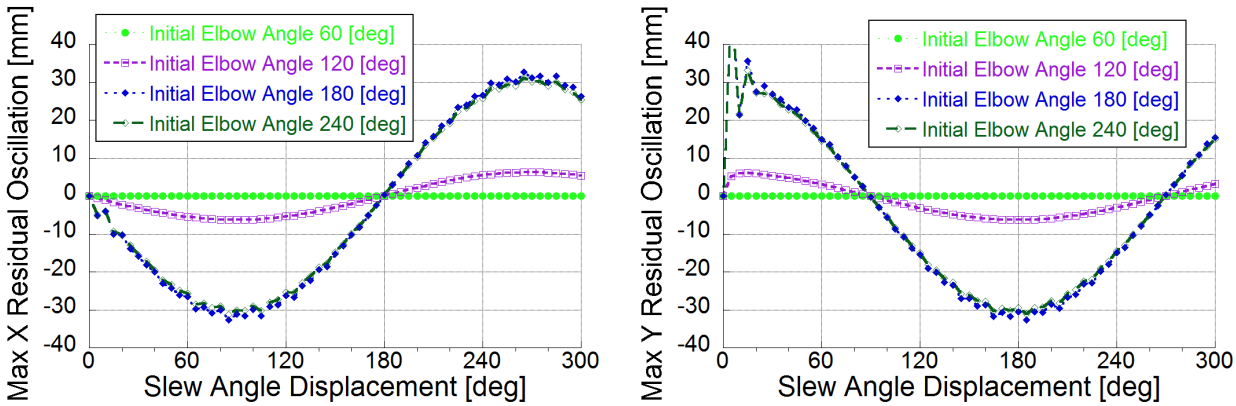

(a) x direction (b) y direction

Figure 55: Maximum residual oscillation in x and y directions for different slew moves and different initial elbow angles.

different slew displacements from 0° to 300° in increments of 5° and initial elbow angles from 0° to 240° in increments of 20°.

The largest residual oscillation is 36 mm in the x direction, 59 mm in the y direction, and 0.5 mm in the z direction. Thus the z direction residual oscillation for slew displacements does not contribute to overall residual amplitude as much as x and y direction residual oscillation. Residual oscillation in z direction for various slew displacements does not oscillate for any initial elbow angle as the residual oscillation in x and y directions.

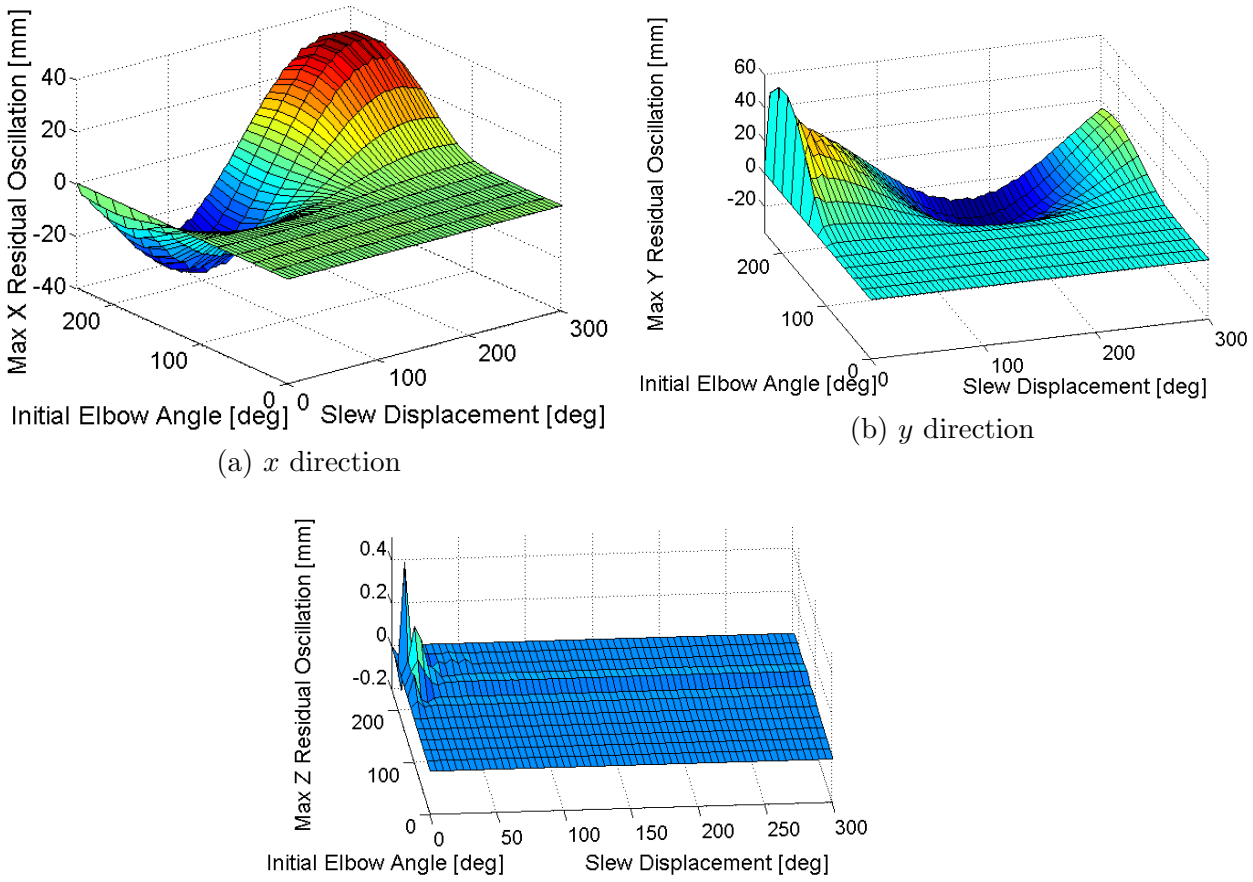

(a) x direction

(b) y direction

(c) z direction

Figure 56: Maximum residual oscillations in x, y, and z directions for different slew displacements and initial elbow angles.

3.3.2 Slewing combined with Elbow Luffing Oscillation

The next step to understanding the dynamics of a cherry picker is to investigate a slewing and elbow luffing move at the same time. For this simulation the slewing move was 160° and the elbow move was 60° while the initial angles of the shoulder and elbow were set to 30° and 160°, respectively. Figure 57 shows the residual oscillation from such a slewing and elbow luffing move in x, y, and z directions. The booms oscillated with a frequency of approximately 1.04 Hz and a damping ratio of 0.14. Maximum displacement of the tip of the arm was 8.34 mm in the x direction, 22.49 mm in the y direction, and 0.01 mm in the z direction.

Figure 59 varies the slewing and elbow luffing moves with the initial shoulder angle at

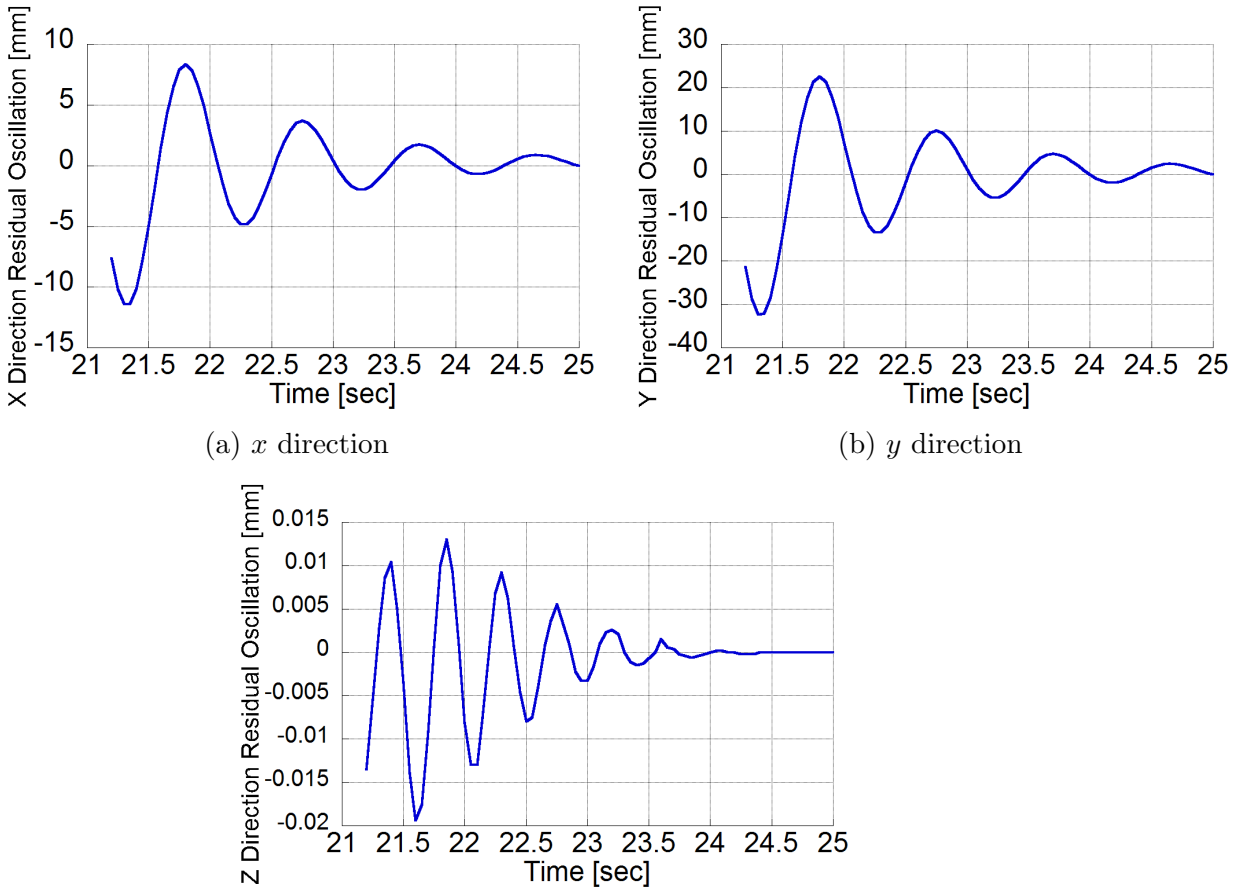

(a) x direction

(b) y direction

(c) z direction

Figure 57: Residual oscillation from a 160° slew and 60° elbow move of a cherry picker.

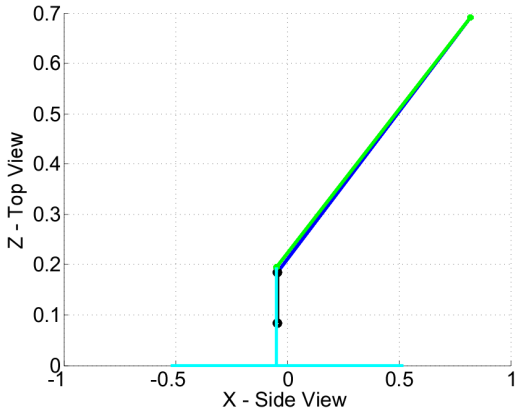

Figure 58: Initial configuration of the cherry picker for the slew and elbow luffing moves.

30° to show the resulting maximum residual amplitude. Slew move was varied from 0° to 180° and elbow move was varied from 0° to 240° both in increments of 20°. Figure 58 shows the initial configuration of the cherry picker for slew and elbow luffing moves.

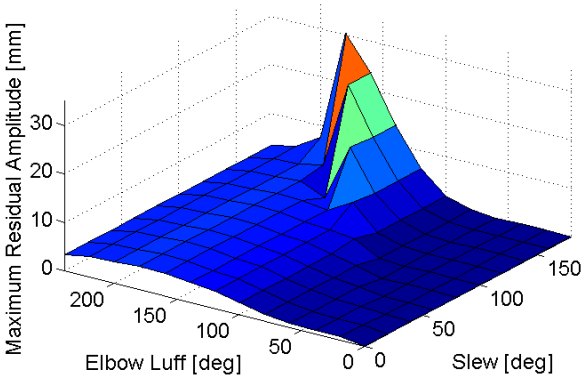

Figure 59: Residual amplitude of slew and elbow luff moves from 0° to 180° and 0° to 240°, respectively.

In general, residual amplitude increases with increasing elbow angle, less compact configurations. Slew moves do not change residual amplitude as much because residual amplitude from slewing moves quickly plateaus. The peak of residual amplitude in the figure is a result of maximum slew move for this case, 180° and maximum extension from the the elbow luff move of 180°; thus centripetal force effected this spike in residual amplitude. Figure 60 shows the cherry picker configurations throughout the moves that generated the largest residual amplitude. Once the elbow angle passes 180°, its non-overcenter limit, the residual amplitude decreases again as overcenter angles are reached. The largest residual amplitude was 30.4 mm and occurred at a slew and elbow move of both 180°.

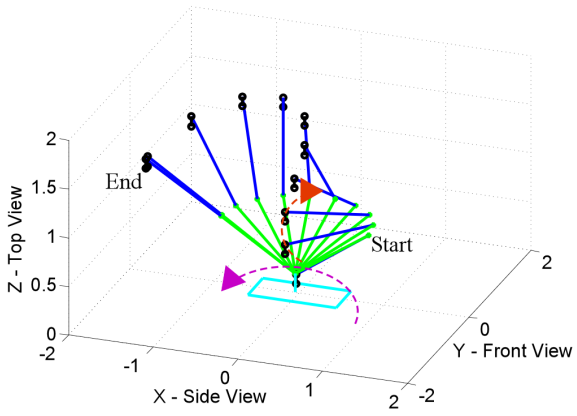

Figure 60: Configurations throughout the moving the slew and elbow luffing angles 180° that generated the largest residual amplitude.

3.4 Slewing Frequencies

Figure 61 shows x, y, and z direction residual oscillation frequencies for initial elbow angle of 120° and different slew displacements from 0° to 300° in increments of 5°. The frequencies range from 1.5 to 2.5 Hz.

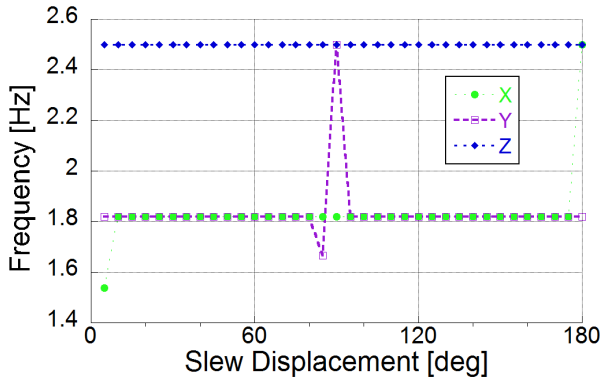

Figure 61: Comparison of frequencies in the x, y, and z directions for different slew moves at a set elbow angle of 120°.

Figure 62 shows the frequencies in the x, y, and z directions for different slew displacements from 0° to 300° in increments of 5° and initial elbow angles of 60°, 120°, 180°, and 240°. For x direction the frequencies ranged from 1 to 4 Hz with more extended elbow angles having lower frequencies ranging from 1 to 2.5 Hz. For y direction the frequencies ranged from 1 to 4 Hz with more extended elbow angles having lower frequencies ranging from 1 to 2.5 Hz. For z direction the frequencies ranged from 2 to 4 Hz with more extended elbow angles having lower frequencies ranging from 2 to 3 Hz. In general the cherry picker has low frequencies for all slew displacements and initial elbow angles except smaller initial elbow angles have slightly higher frequencies.

3.5 Input Shaping to Reduce Oscillation

Many have successfully used types of control systems to eliminate oscillation of flexible systems, such as concrete placing boom [2], model boom crane [12, 13, 11], and aerial lifts [6, 9, 10]. One particular aerial lift control article [9] used a specific input shaping control system [8] to suppress two-modes in the residual oscillation. For this model, the simple ZV shaper introduced in Chapter 1 will be utilized to eliminate oscillation induced

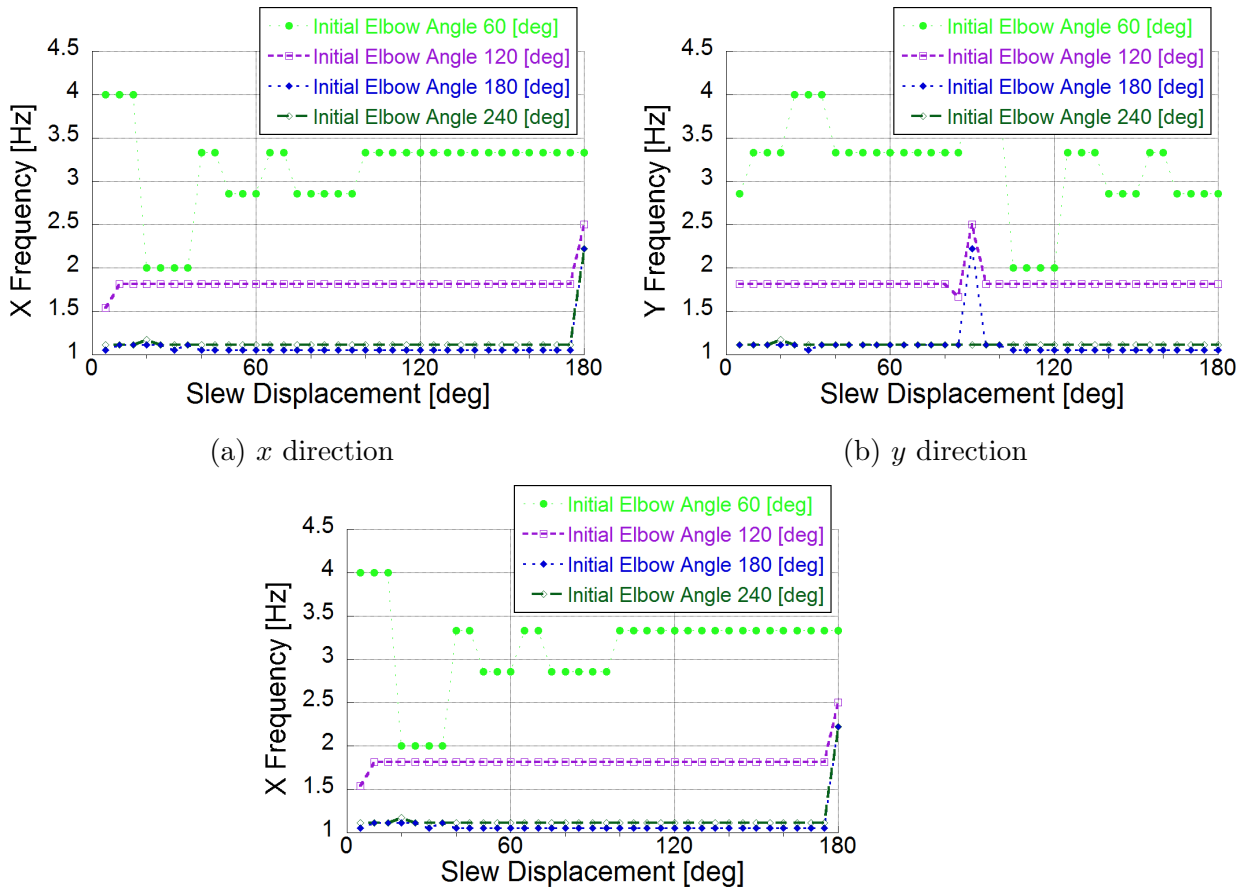

(a) x direction

(b) y direction

(c) z direction

Figure 62: Frequencies in x, y, and z directions for different slew displacements and initial elbow angles.

by machine-motion.

For the previous 160° slewing move conducted with initial shoulder angle of 30° and initial elbow angle of 160°, the oscillation frequency was 1.21 Hz with a damping ratio of 0.155. Using this information the following ZV shaper of amplitudes A_i and times t_i was calculated:

$$\begin{bmatrix} A_i \\ t_i \end{bmatrix} = \begin{bmatrix} 0 & 0.6208 \\ 0.4183 & 0.3792 \end{bmatrix} \tag{17}$$

Convolving this input shaper with the desired slewing trapezoidal velocity profile resulted in much lower residual oscillations. Figure 63 compares the unshaped residual oscillation of the slew move to the shaped residual oscillation for both x and y directions.

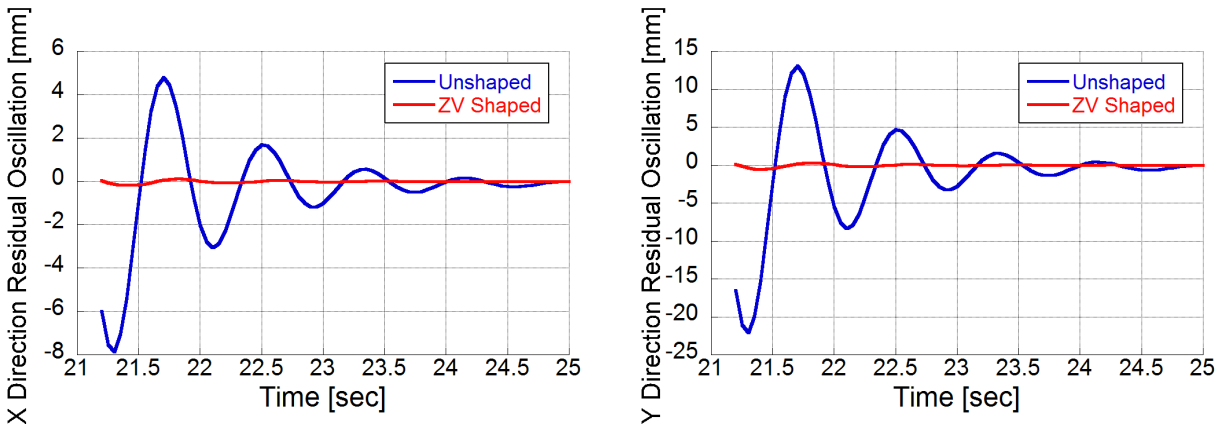

(a) x direction (b) y direction

Figure 63: Comparison of shaped and unshaped residual oscillation from a 160° slew move of a cherry picker.

The maximum displacement of the tip of the arm dropped to 0.12 mm in the x direction, a 97% reduction, and 0.32 mm in the y direction, a 98% reduction, with the shaped input command.

For the previous 160° slewing and 60° elbow luffing move conducted with initial shoulder angle of 30° and initial elbow angle of 160°, the oscillation frequency was 1.04 Hz with a damping ratio of 0.14. Using this information the following ZV shaper of amplitudes A_i and times t_i was calculated:

$$\begin{bmatrix} A_i \\ t_i \end{bmatrix} = \begin{bmatrix} 0 & 0.6093 \\ 0.4856 & 0.3907 \end{bmatrix} \tag{18}$$

Convolving this input shaper with the desired trapezoidal velocity profile of that slew and elbow luff move resulted in much lower residual oscillations. Figure 64 compares the unshaped residual oscillation of the slewing move to the shaped residual oscillation for x, y, and z directions. Maximum displacement of the tip of the arm dropped to 0.25 mm in the x direction, a 97% reduction, 0.7 mm in the y direction, a 97% reduction, and 0.003 mm in the z direction, a 75% reduction, with the shaped input command.

To show a wide scale effect of input shaping on a system's residual amplitude, the simulation of varied slewing and elbow luffing moves was input shaped using a ZV shaper for a frequency of 1.1 Hz and damping ratio of 0.14:

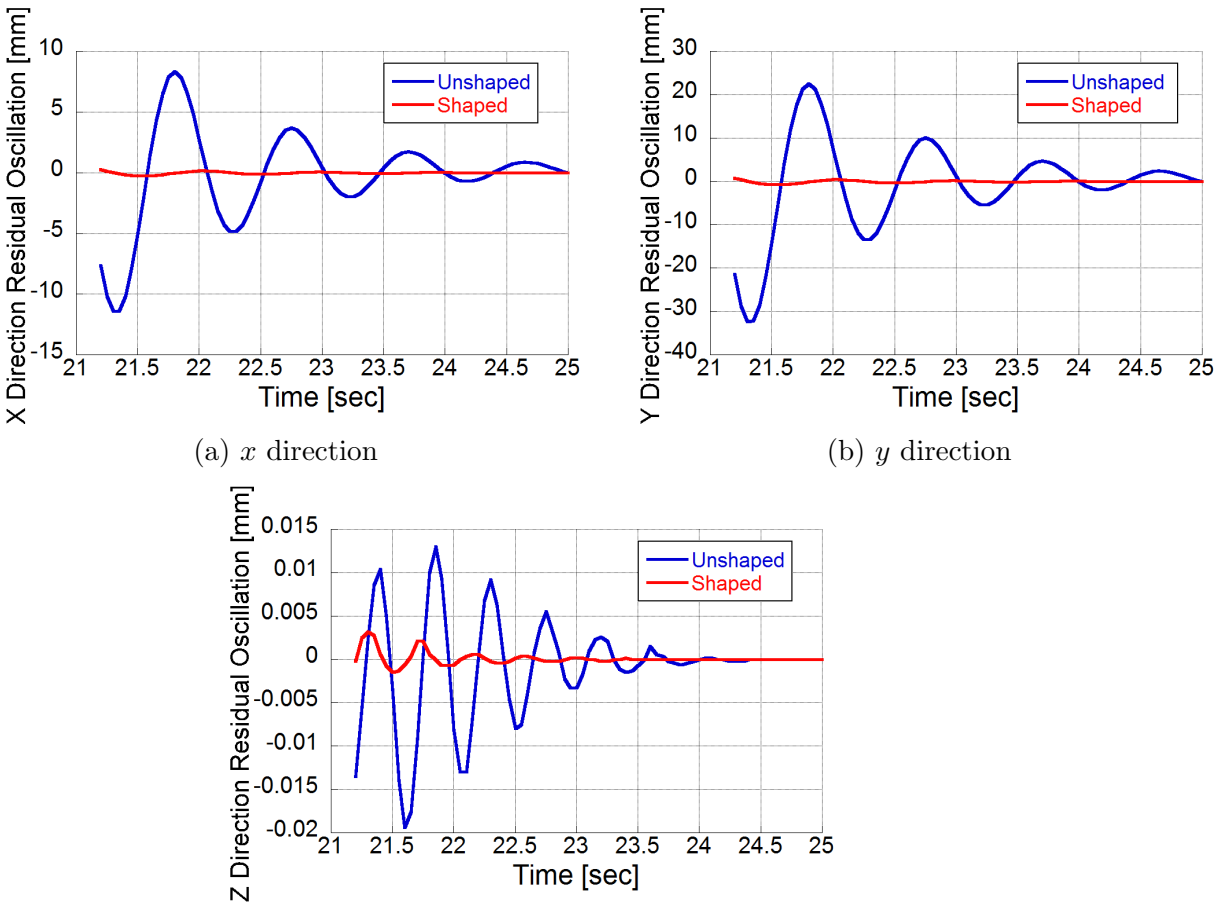

(a) x direction

(b) y direction

(c) z direction

Figure 64: Comparison between shaped and unshaped residual oscillation from a 160° slew and 60° elbow move of a cherry picker.

$$\begin{bmatrix} A_i \\ t_i \end{bmatrix} = \begin{bmatrix} 0 & 0.6093 \\ 0.4591 & 0.3907 \end{bmatrix} \tag{19}$$

Figure 65 shows input shaping greatly reduced residual amplitude over all slew and elbow moves. The maximum residual amplitude from input shaped is 4.23 mm, 86% reduction, and overall residual amplitude was reduced by 76%.

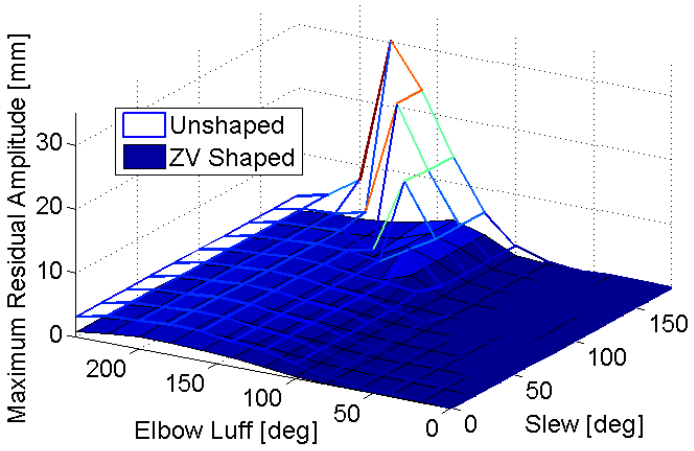

Figure 65: Comparison between shaped and unshaped residual amplitude of slew and elbow luff moves from 0° to 180° and 0° to 240°, respectively.

3.6 Summary

Overcenter configurations decrease residual amplitude in luffing and slewing moves. Slewing moves result in quick plateauing of residual amplitude. At extended configurations, slewing moves see two-mode oscillations and greater residual oscillations. Overall residual amplitude for slewing moves are generated from residual oscillations in the x and y directions. Cherry picker generally how low frequencies ranging from 1 to 3 Hz that does not change much over slew displacement but does increase slightly when at smaller elbow angles. Input shaping can reduce of the residual oscillation caused by slewing moves as well as combined slewing and elbow luffing moves.

CHAPTER IV

TIP-OVER ANALYSIS OF DOUBLE-BOOM ARTICULATING AERIAL LIFTS

The previous chapter showed how flexibility of articulating aerial lifts induce oscillation. This chapter will focus on the tip-over instability of articulating aerial lifts. The static tip-over analysis described here in sections 2.1.1 - 2.1.3 is work performed by Dr. Joshua Vaughan and Dr. William Singhose for an aerial lift accident that occurred in Boston, MA. That work is extended by investigating the effects of payload mass in section 2.1.4. Section 2.2 then presents a dynamic tip-over stability analysis.

4.1 Static Telescopic Articulating Aerial Lift Tip-Over

4.1.1 Stability Model

The model in Figure 66 was used to analyze the stability of the Grove A125J articulated telescoping aerial lift. The top portion of the base rotates with respect to the fixed base according to slew angle θ, as shown by the TOP VIEW in Figure 66. The links of the aerial lift are labeled in order from LA to LG according to their distance along the chain of links away from the base. A point mass, M, is included at the end to represent the platform load, such as operators and tools.

The riser arm, LA, rotates upward from the base by θ_L. Link LB is the portion of the riser that telescopes outward. The mast, represented by Link LC, remains vertical in all orientations. LD and LE represent the boom and boom extension links. Link LF rotates away from horizontal according to θ_B, in order to keep the basket link, LG, horizontal in all orientations. The boom arm rotates from horizontal according to angle θ_U. The extension distance of the riser arm is represented by ΔLow, and the upper boom extension is represented by ΔUp.

4.1.2 Parameter Determination

Figure 67 was used to determine the link lengths. The figure was acquired from the operators manual and assumed to be drawn to scale. Lengths of links that were not labeled in the official documentation figure were calculated using the scaling derived from those that were labeled. These approximated values are shown by large red numerical labels.

The mass properties were selected according to information from the Grove repair manual, including link masses, actuator masses, and total system mass. As a check on the mass distribution between the various components, the Center of Mass (COM) of the model was compared to that given in the official literature. The COM location of the machine in the contracted state in the official literature is shown in Figure 68. The modeled location of the COM in the same configuration is shown in Figure 69. The modeled valued of the COM only varies from the value given in the official literature by approximately 5 inches in the vertical direction and 6 inches in the horizontal direction.

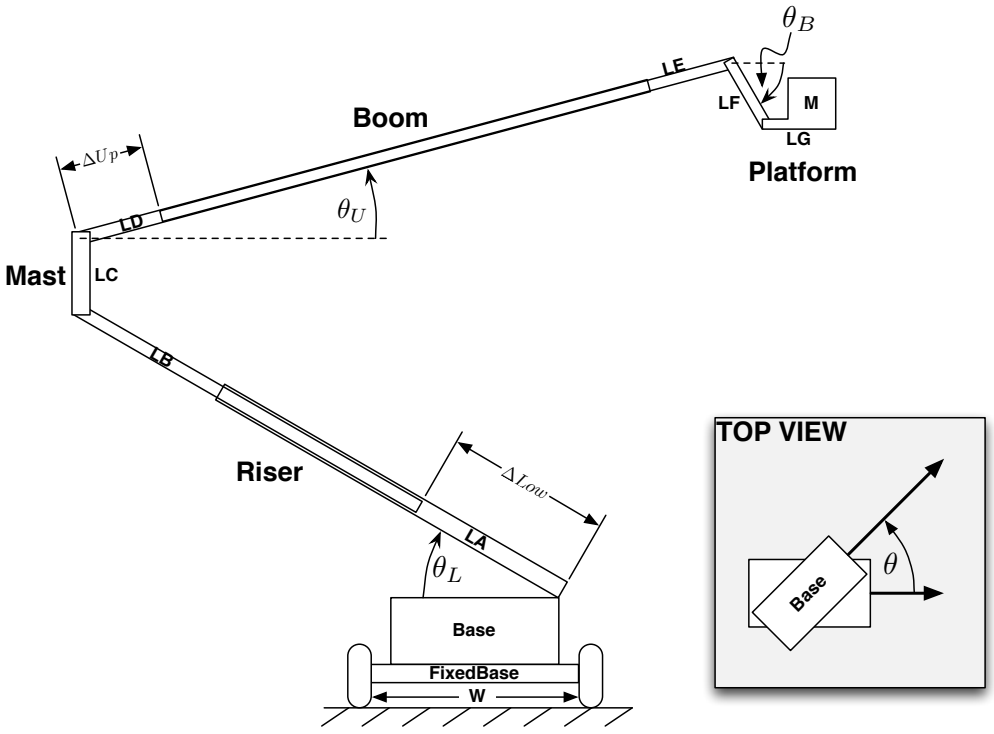

Figure 66: Model of the Grove A125J Articulated Telescoping Aerial Lift.

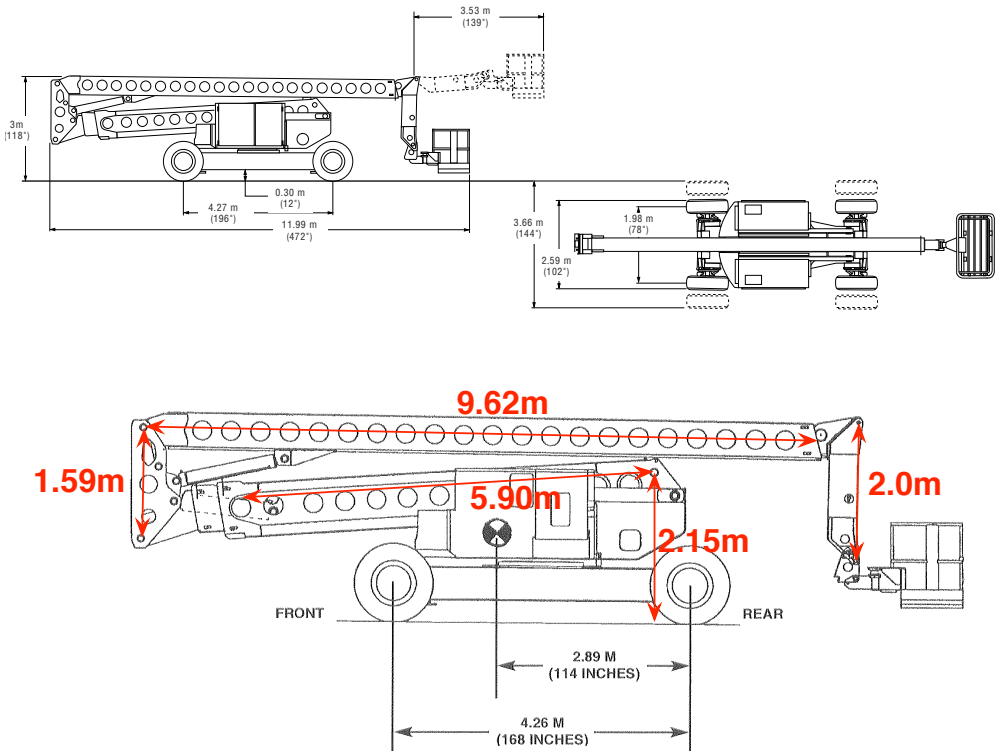

Figure 67: Machine Dimensions (Red Indicates Calculated Lengths)

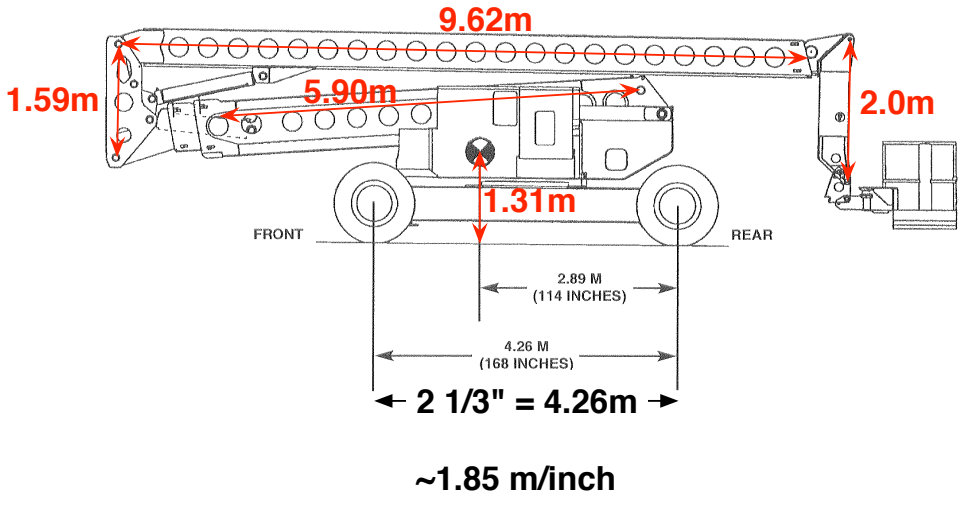

Figure 68: COM Location in Official Literature

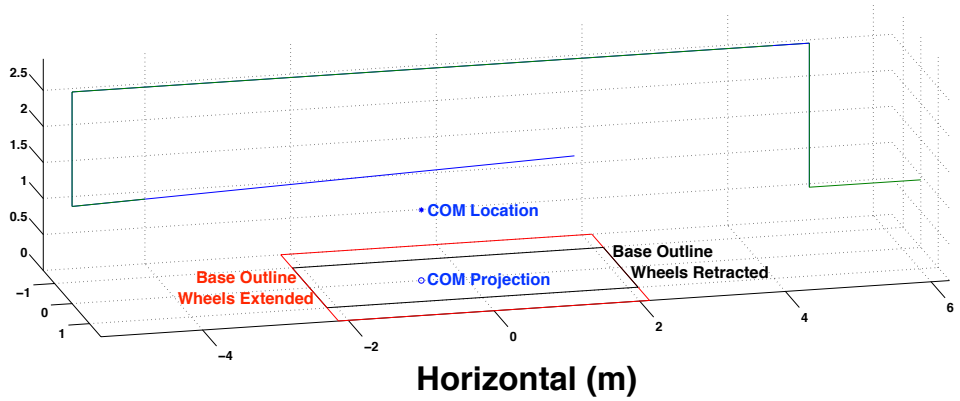

Figure 69: Simulated COM Location

4.1.3 Stability

Stability of this system was analyzed for a horizontally-flat base condition. The system was considered stable when the system center-of-mass (COM) was contained within the support rectangle defined by the four tire ground-contact locations. The effective tire-ground contact locations were approximated as the center of the tire footprint on the ground. The support polygons are shown in Figure 69 for both the wheels extended and contracted states.

The angles of each arm joint and the telescoping extension length of the riser and boom were varied throughout their feasible ranges. At each configuration, the stability was determined and recorded in a database. The data was recorded by saving the platform position for each configuration and a flag indicating whether or not it was stable.

Note that many platform positions can be achieved using multiple combinations of link positions and angles. For example, Figure 70 shows that the platform can be positioned low and near the base using two different extension lengths of the riser and boom. In Figure 70(a), the platform is positioned using a compact configuration of the riser and boom. In Figure 70(b), the same platform position is obtained using a more extended configuration of the riser that is counteracted by a more extended configuration of the boom. The stability properties of these two configurations are not the same. Therefore, simply indicating a platform position does not reveal whether or not the machine is stable. The entire configuration of the machine must be known in order to determine stability.

The stability of the two configurations in Figure 70 is schematically represented in Figure 71. In Figure 71(a), both the riser and boom arms are unextended and the system

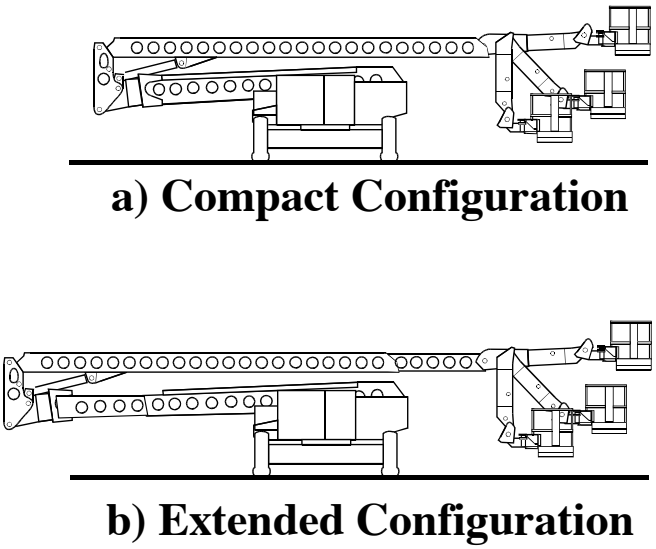

Figure 70: Two Different Configurations that Produce the Same Platform Position

COM, indicated by the circle, is nearly centered within the support rectangles. The smaller black rectangle is for the wheels-contracted state, and the larger red rectangle is the base of

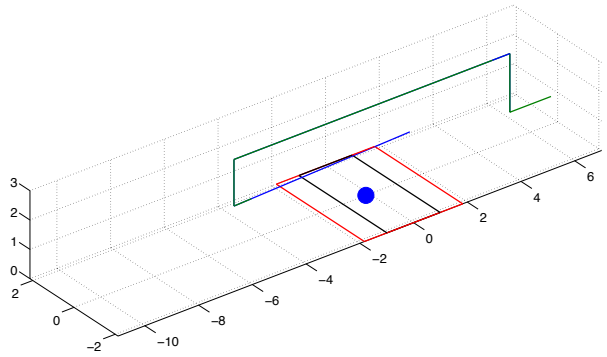

(a) Compact Configuration

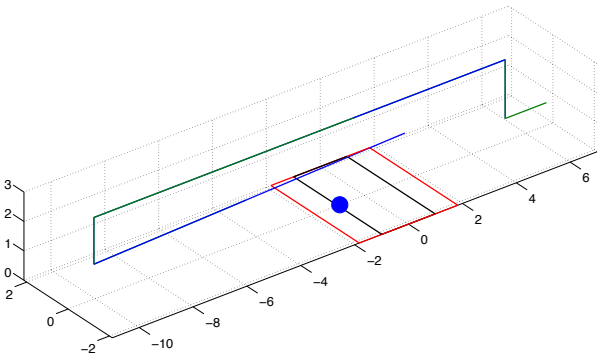

(b) Extended Configuration

Figure 71: Configuration-Dependent Stability

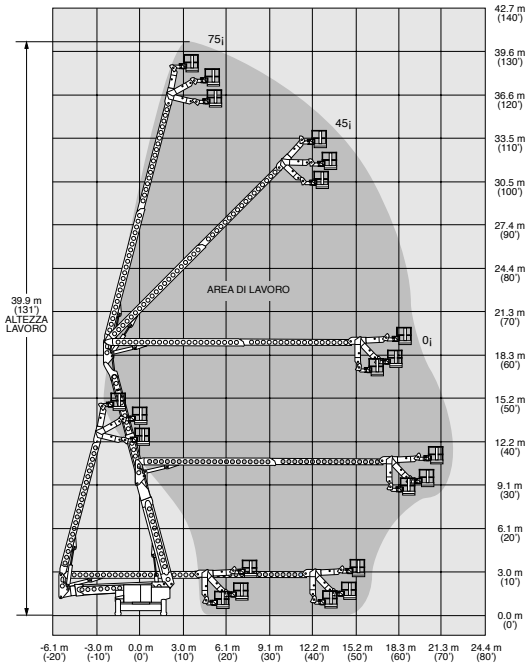

Figure 72: "Advertised" Stable Work Area [3]

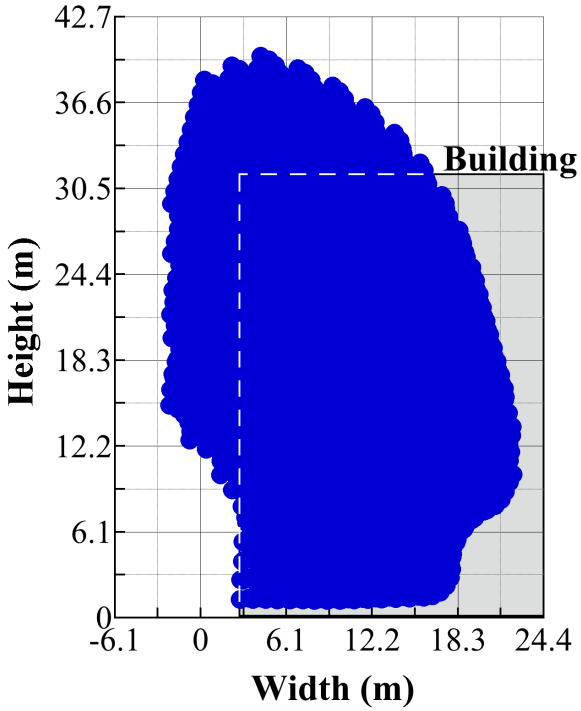

Figure 73: Potentially-Stable Model Area

support for the wheels-extended state. Figure 71(a) indicates that the machine is in a very stable condition when the riser and boom are in the compact configuration corresponding to Figure 70(a). However, in Figure 71(b), the system is considerably less stable. Even though the endpoint is in an identical location, the COM has moved away from the center of the support rectangle, to the left in the figure. It is now on the edge of stability for the wheels-contracted case.

Figure 72 shows the stable workspace as indicated in the official machine literature [3]. Note that only the platform position is used to indicate whether or not the machine is stable. This diagram oversimplifies the stability properties of the machine. The dark area *can be* stable, but only if the interlock system is functioning properly and does not allow the machine to position the platform using the many alternative configurations that could be used to achieve the same platform position.

Figure 73 shows the potentially-stable work area determined by the stability model, with the wheels extended. The potentially-stable workspace calculated from the model closely matches that from the official literature. It is slightly larger because it includes stable points

that the interlock system would not allow the machine to reach.

Figure 74 shows the approximate distance of the building edge from the machine during operations that preceded the accident. Using this information, an approximate building location can be overlaid on the workspace. This is shown for a 72° riser angle in Figure 75(a). As shown, the system is stable over the entire reachable workspace with the riser fixed at this angle and the wheels extended. If the wheels are retracted, then there are areas where the system can be unstable, as shown in Figure 75(b).

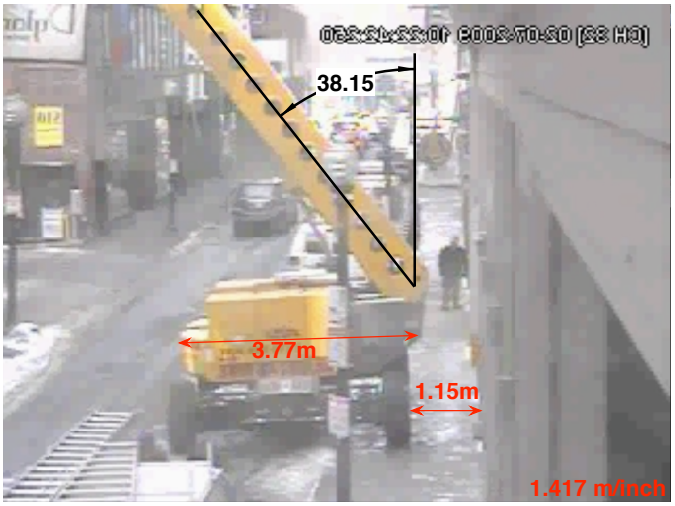

Figure 74: Building Location Relative to the Device (Image Mirrored from Video)

However, there are still large areas of the "safe" workspace that are not stable if the machine reaches those positions through an alternative configuration of the link lengths and angles. For example, Figure 76 illustrates two configurations that reach the same platform position. The stable configuration results in the COM being located within the support rectangle, between the wheels. However, the unstable case results in the COM being outside of the vehicle wheel base. This condition would cause the machine to tip over.

The results in Figures 75-76 clearly demonstrate that the interlock system must operate perfectly in order to ensure safe operation. If the interlock system does not function perfectly at all times, then the machine can easily go unstable and tip over.

Figures 77–80 further demonstrate the machine's potential instabilities. Figure 77 shows the platform positions that can be reached in a stable manner. Figure 78 shows the positions

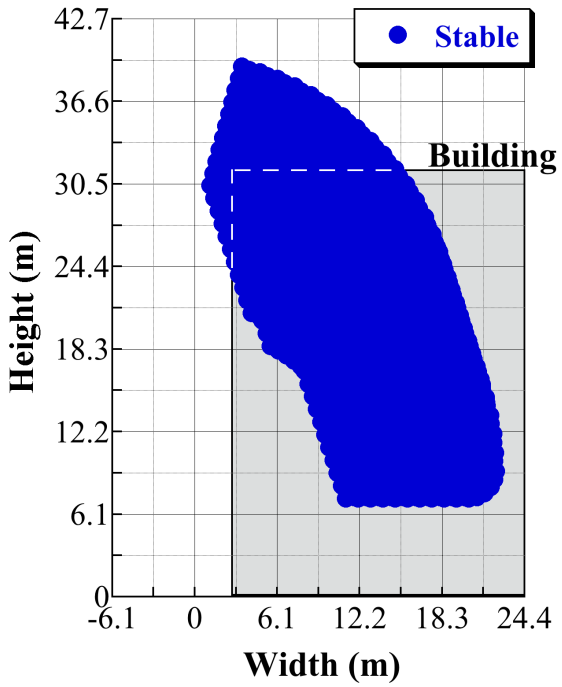

(a) Wheels Extended

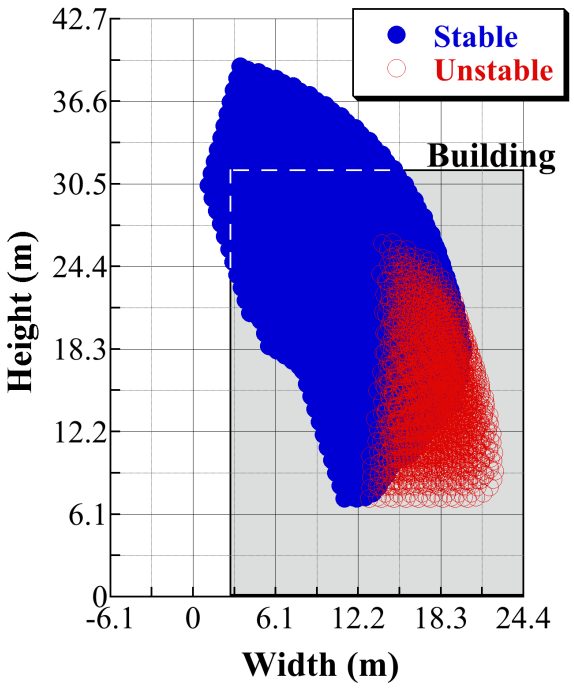

(b) Wheels Retracted

Figure 75: Workspace with Riser Fixed at 72°

that can be reached in an unstable condition. Notice that there is a significant overlap between Figures 77 and 78. Figure 79, shows platform endpoint locations in the workspace

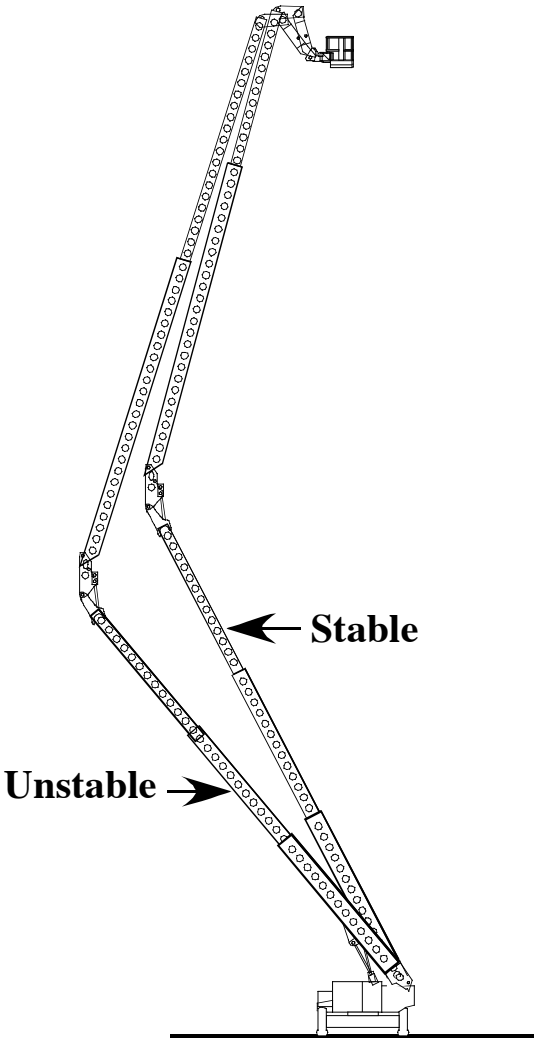

Figure 76: Examples of Stable and Unstable Configurations Reaching the same Platform Location.

where the stability is dependent upon the link lengths and the angles. These places can be reached in both stable and unstable configurations. Figure 80 overlays the three different conditions of stability.

4.1.4 Effects of Added Mass on Platform

Using the simulation of the telescopic articulating aerial lift, the effects of increased platform mass was investigated. Two different masses, 500 kg and 1000 kg, were simulated as the platform mass. Figure 81 shows both the unstable and stable platform locations for platform masses of 500 kg and 1000 kg. Figure 82 shows only the unstable platform locations for a

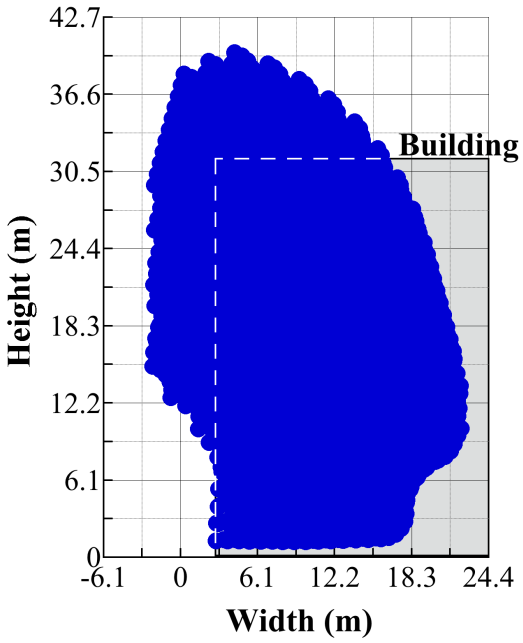

Figure 77: Potentially-Stable Platform Locations

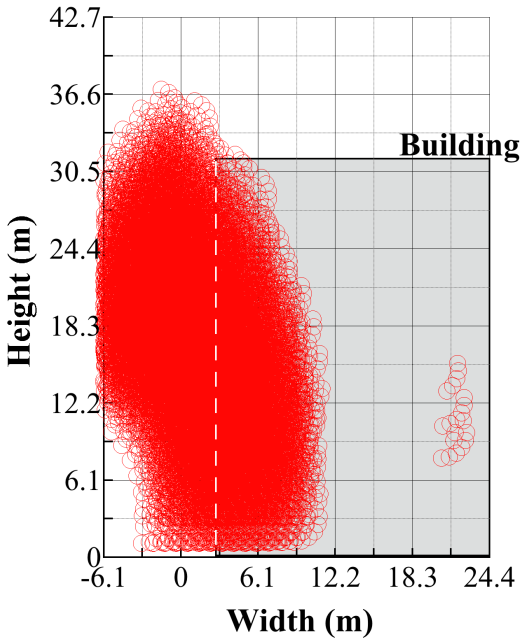

Figure 78: Potentially-Unstable Platform Locations

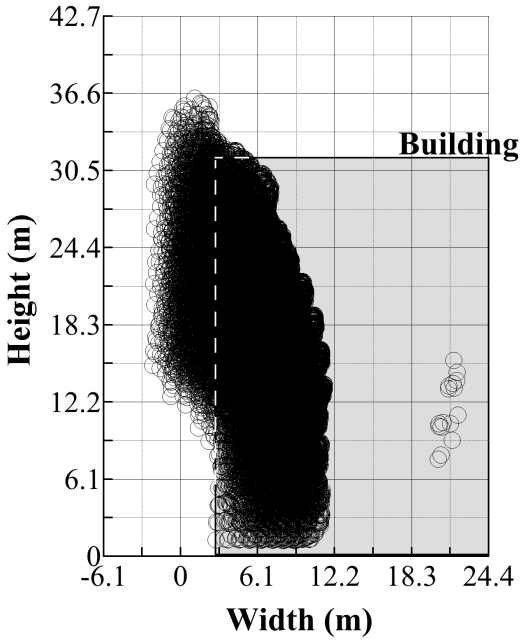

Figure 79: Points that Can Be Either Stable or Unstable

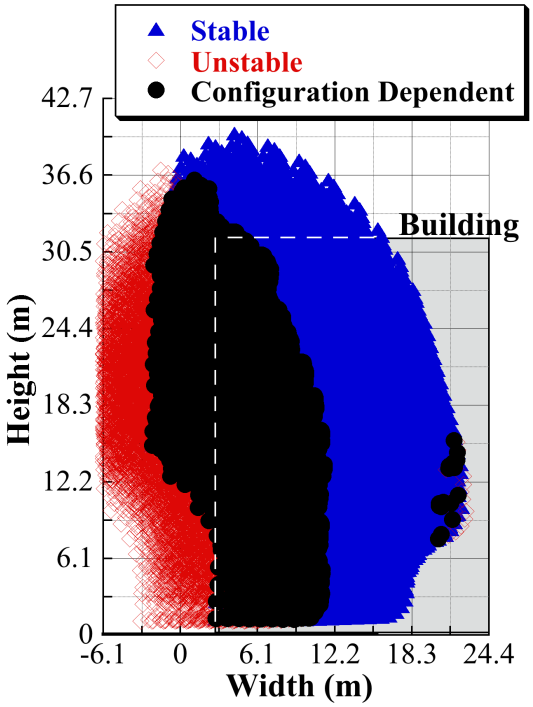

Figure 80: Demonstrating Configuration Dependent Stability

platform mass of 500 kg. Lastly, Figure 83 shows only the unstable platform locations for a platform mass of 1000 kg. By increasing platform mass from 225 kg to 500kg and from

500 kg to 1000 kg, the number of unstable platform locations increases both to the right and left of the aerial lift.

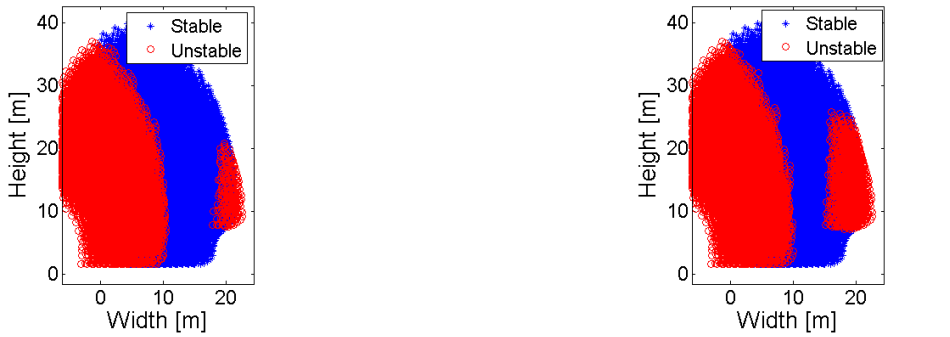

(a) Platform mass 500 kg (b) Platform mass 1000 kg

Figure 81: Potentially stable and unstable platform locations for platform masses of 500 kg and 1000 kg.

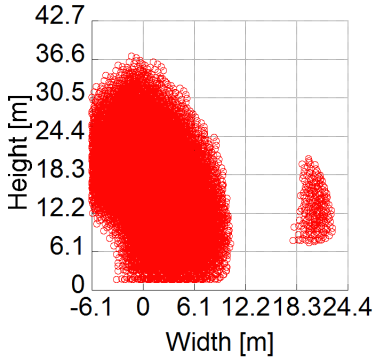

Figure 82: Potentially unstable platform locations for a platform mass of 500 kg.

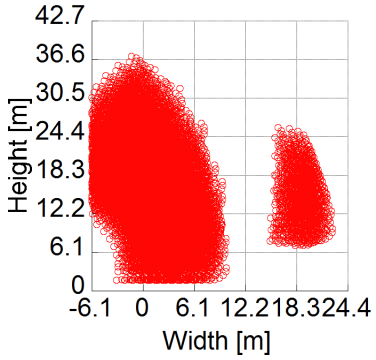

Figure 83: Potentially unstable platform locations for a platform mass of 1000 kg.

4.2 Dynamic Model Articulating Aerial Lift

4.2.1 Tip-Over Stability Margin

Determining when the cherry picker tipped over was accomplished by a tip-over stability margin method (Force-Angle Stability Margin) introduced by Papadopoulos [16]. The tip-over stability margin is designed for mobile manipulators. Manipulators are considered to be parts on top of the vehicle that can change their overall center of mass by changing orientations, similar to an aerial lift. Instead of simply depending on the distances to the edges of the support base, the tip-over stability margin is height sensitive which is needed for the analysis of an aerial lift because aerial lifts are used at high heights giving them their vulnerability to tipping over. The method begins by defining the support polygon or ground contact locations projected onto a horizontal plane. Ground contact points of the support polygon, p_i, are expressed as:

$$p_i = [p_x \;\; p_y \;\; p_z]_i^T, \qquad i = 1, \ldots, n. \tag{20}$$

The final ground contact point is p_n. In addition, p_c is the vehicle's center of mass. The Force-Angle Stability Method creates a tip-over margin by using all forces and moments about the system's center of mass. For this method, stability is measured as the angle between the net force vector, f_r, and each of the tip-over axis normals, l. Possible tip-over mode axes are numbered in clockwise order, as shown in Figure 84, and given by:

$$a_i = p_{i+1} - p_i \qquad i = 1, \ldots, n-1 \tag{21}$$

The last tip-over mode axis, a_n, is defined by:

$$a_n = p_1 - p_n \tag{22}$$

There are four tip-over axes for the cherry picker, a truck-mounted aerial lift: the front, the back, and the right and left sides of the truck. Tip-over axis normals that intersect the vehicle's center of mass are subtracted from $(p_{i+1} - pc)$ which lies along $\hat{a}_i$. Letting $\hat{a} = a/\|a\|$, the axis normals are:

$$l_i = (I - \hat{a}_i \hat{a}_i^T)(p_{i+1} - p_c), \tag{23}$$

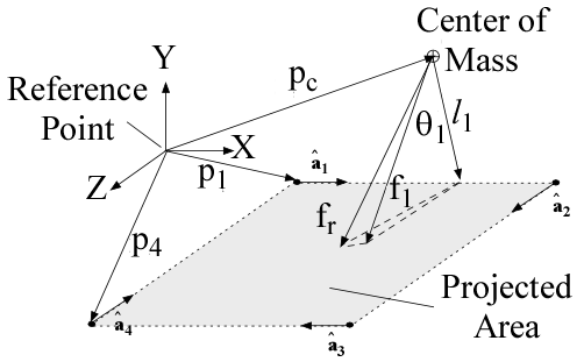

Figure 84: General 3D tip-over stability margin geometry [4].

where I is a 3x3 identify matrix.

The net force, f_r, acting on the center of mass consists of forces that could cause tip-over instability: gravitational forces, external disturbances, reaction forces, and forces transmitted by the manipulator. Reaction forces for not contribute to tip-over instability. For a given tip-over axis, $\hat{a}_i$, the components of the net force acting about the tip-over axis:

$$f_i = (I - \hat{a}_i \hat{a}_i^T) f_r \tag{24}$$

The same procedure is implemented on the net moments, n_r, acting about the center of mass; thus, components of the net moment about the tip-over axis:

$$n_i = (\hat{a}_i \hat{a}_i^T) n_r \tag{25}$$

Figure 85 shows the force couple, $f_{n,i}$, acting on the center of mass by:

$$f_{n,i} = \frac{\hat{l}_i \times n_i}{\|l_i\|} \tag{26}$$

Normalized l is $\hat{l} = l/\|l\|$. Thus, the net force vector, f_i^*, is:

$$f_i^* = f_i + f_{n,i} = f_i + \frac{\hat{l}_i \times n_i}{\|l_i\|} \tag{27}$$

Normalized f_i^* is $\hat{f}_i^* = f_i^*/\|f_i^*\|$. The tip-over margins, angle between the net force vector and each of the tip-over axis normals, are determined by:

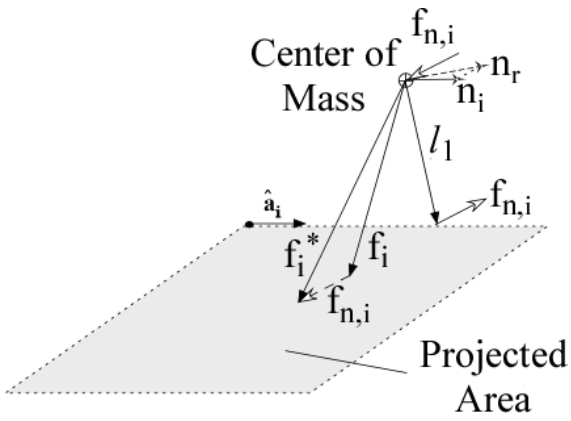

Figure 85: Equivalent force couple at the center of mass [4].

$$\theta_i = \sigma_i \cos(\hat{f}_i^* \cdot \hat{l}_i)^{-1}, \quad i = 1, \ldots, n. \tag{28}$$

σ_o in the original tip-over stability margin specified the sign of θ_i. However, for the cherry picker tip-over stability margin, the magnitude of θ_i when it is negative, which is when the object is tipping over, is not of necessity [4]. Thus, only positive magnitudes of θ_i define the tip-over stability margin and the value of zero takes place of all negative magnitudes denoting the object will tip-over or is already tipped over. In addition, only the minimal tip-over stability margin is outputted because only the minimal margin is of importance for this analysis. For this method, the highest tip-over margin, the greatest stability, occurs close to the geometric center and at a low center of gravity.

4.2.2 Stability Analysis

An important aspect of a cherry picker's tip-over margin is the location of the center of mass. A cherry picker of similar configuration to the experimental model, has the rotating tower longitudinally closer to one side of the base. From a static and pseudo-dynamic model of the cherry picker, the tip-over stability margin determined that the cherry picker is most likely to statically tip-over with the booms completely extended over the side of the base with the rotating tower [5]. For the cherry picker modeled in Chapter 3, the rotating tower is located a distance away from the center of the base, to the backside of the aerial lift's base. Thus, the backside of the base is shorter in comparison to the front side given the location of the rotating tower. Placing the rotating tower off-centered reduces stability on

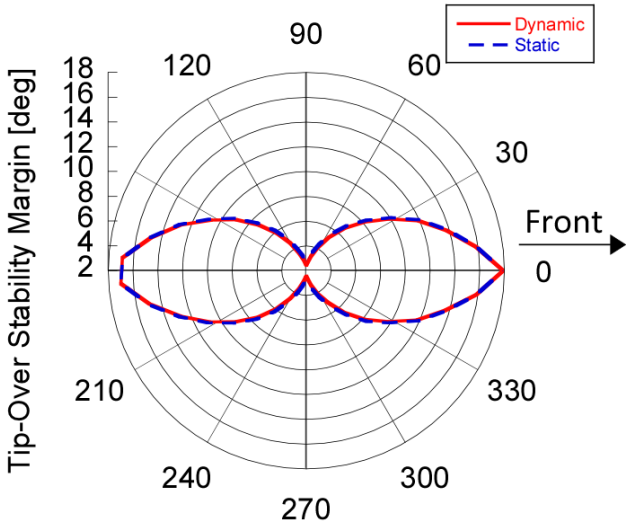

Figure 86: Comparison between dynamic and static tip-over stability margin.

the quadrants of the base it resides because the payload is brought closer to the edges of the support base as it slews over to those quadrants. Other likely static tip-over configurations are when the booms are fully extended to either side of the aerial lift, parallel to it's lateral axis. When the joint angles move into a more compact form, the static tip-over margin increases meaning it is less likely to tip-over [4].

With the same articulating aerial lift model presented in Chapter 3, tip-over margin of a dynamic cherry picker was analyzed. Figure 86 shows the dynamic tip-over stability margin compared to static tip-over stability margin for an initial set shoulder angle of 65°, initial set elbow angle of 160°, and slew displacements from 0° to 360°. Dynamic is due to the simulated cherry picker's flexibility and ability to move to the location, thus the tip-over margin stated at a slew displacement of 30° is the least tip-over margin at the end of moving the cherry picker from the slew angle of 0° to the slew angle of 30°. Previously, tip-over margin of a cherry picker was only semi-dynamic compared to static. The front of the cherry picker is at slew angle of 0°. In the figure, the dynamic margin is slightly inside of the static margin.

An effect that was not previously investigated is the change of platform mass on the tip-over stability margin. Figure 87 uses the same previous set initial angles, the same slew displacements, and changing the platform mass from 2 kg to 3 kg to 4 kg. By increasing

the platform mass the tip-over stability margin decreases meaning the aerial lift is closer to tipping over. Increasing platform mass reduces stability of an aerial lift. The front of the cherry picker is at slew angle of 0°.

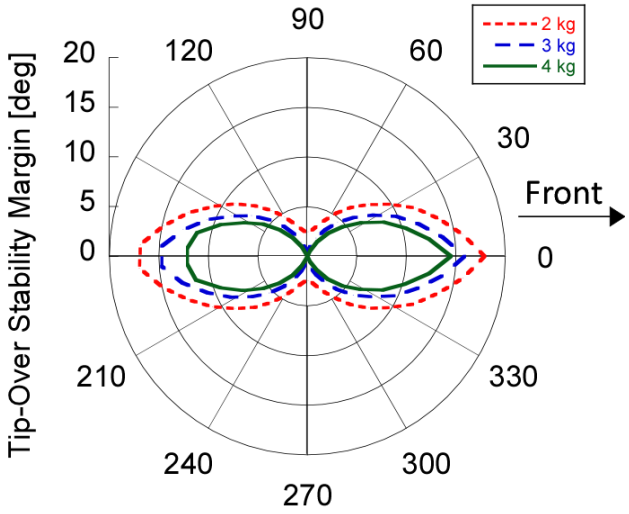

Figure 87: Comparison of dynamic tip-over stability margin for added platform mass.

Chapter 3 reviewed some effects of oscillation of overcenter configurations. To compare an overcenter configuration tip-over stability margin to a non-overcenter configuration tip-over stability margin, an overcenter configuration was chosen and non-overcenter configurations with the same end location were determined using basic geometry. The chosen overcenter configuration is a shoulder angle of 85° and elbow angle of 200°. The resulting non-overcenter configurations are a shoulder angle of 75°, elbow angle of 180°, and a shoulder angle of 65°, elbow angle of 160°. Figure 88 shows the chosen overcenter configuration and the resulting non-overcenter configurations.

Figure 89 shows the overcenter configuration has the greatest tip-over stability margin. All non-overcenter configurations have less tip-over stability margins compared to the overcenter configuration. The configuration with the second highest shoulder angle has the second highest tip-over stability margin because the lower boom closer to the base's center of mass increases stability. The front of the cherry picker is at slew angle of 0°.

For overcenter configurations with the same platform location as a non-overcenter configuration, the lower boom must be brought higher, bringing the lower boom closer to the

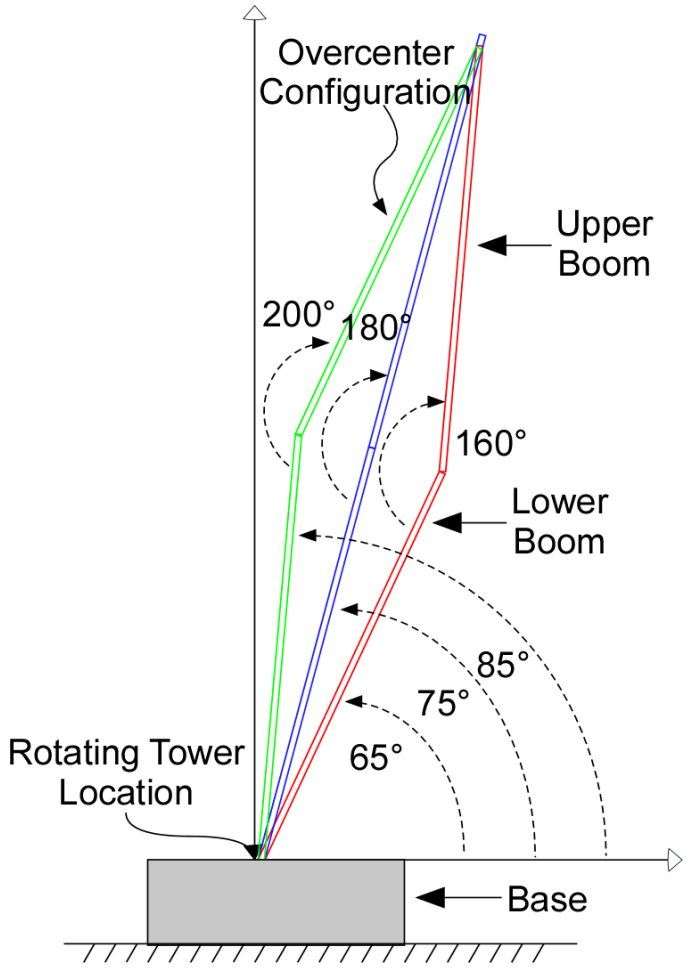

Figure 88: Overcenter and non-overcenter configurations with the same end location.

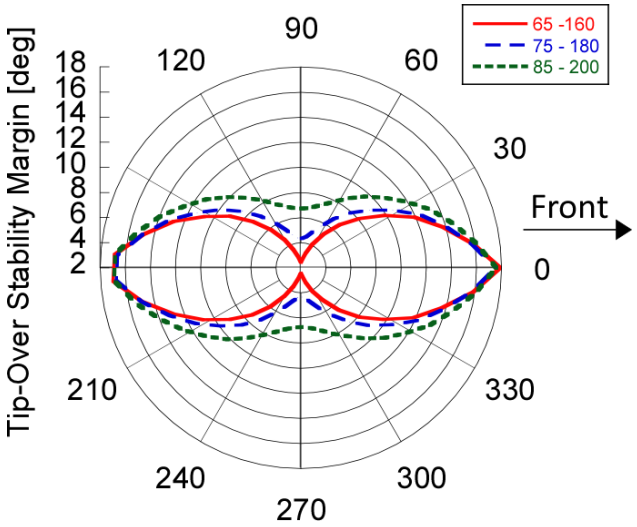

Figure 89: Comparison of dynamic tip-over stability margin for overcenter and non-overcenter configurations with the same end location.

center of the support base and the upper boom must be brought lower to match the same platform location, as seen in the comparison of configurations Figure 88. Thus, the center of mass of an aerial lift in an overcenter configuration is brought closer to and above the center of the support base, a location of greater stability. Hence, overcenter configurations are stabler than non-overcenter configurations.

Figure 90 shows the overcenter configuration as having the least amount of residual amplitude. All non-overcenter configurations have greater residual amplitude compared to the overcenter configuration. The configuration with the second highest shoulder angle has the second lowest residual amplitude. The front of the cherry picker is at slew angle of 0°. As shown in Chapter 3, after a certain slew displacement the residual amplitude plateaus which occurred for all configurations.

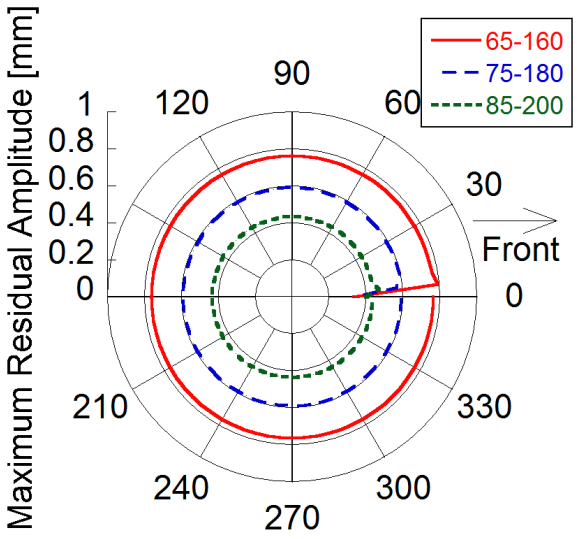

Figure 90: Comparison of slewing-induced residual amplitude for overcenter and non-overcenter configurations with the same end location.

4.3 Experimental Setup and Maximum Static Payload Mass

An experimental model of a cherry picker previously built was used to determine the maximum static payload mass at multiple slew angles while in the configuration of 0° shoulder angle and 180° elbow angle. The width of the platform was also varied. The weights of the experimental cherry picker are listed in Table 9 and the dimensions are listed in Table 10.

Table 9: Cherry picker experimental weights in kilograms.

Part	Weight
Leg	0.308
Base	19
Rotating tower	6.98
Counterweight	6.27
Lower boom	1.75
Upper boom	1.5

Table 10: Cherry picker experimental dimensions in meters.

Description of dimension	Length
Leg height	0.1778
Base length	0.99
Base height	0.083
Distance to x center of mass of base from center of base	0.13
Distance to y center of mass of base from center of base	0.1
Distance to rotating tower in x direction from center of base	0.134
Rotating tower height	0.381
Distance to y center of mass of actuator on rotating tower and counterweight	0.102
Distance to x center of mass of the counterweight	0.23
Lower boom length	0.92
Upper boom length	0.88

The counterweight is located on the opposite side of the lower boom above the rotating tower as well. The counterweight rotates according to the slew of the rotating tower and the luff of the lower boom. There is an actuator halfway up the rotating tower that also rotates according to the slew of the rotating tower. The original width of the base is 0.43 meters. Figure 91 shows the maximum static payload mass for the original width of the base and experimental points for certain slew angles. Experimental results are similar to simulation results. Experimental points were not collected for slew angles that required great amount of weight to tip-over the experimental setup and could potentially break parts of the experimental setup before the cherry picker tipped over. The side of the cherry picker that was tested has a lesser amount of weight necessary to tip-over than the other side of the cherry picker.

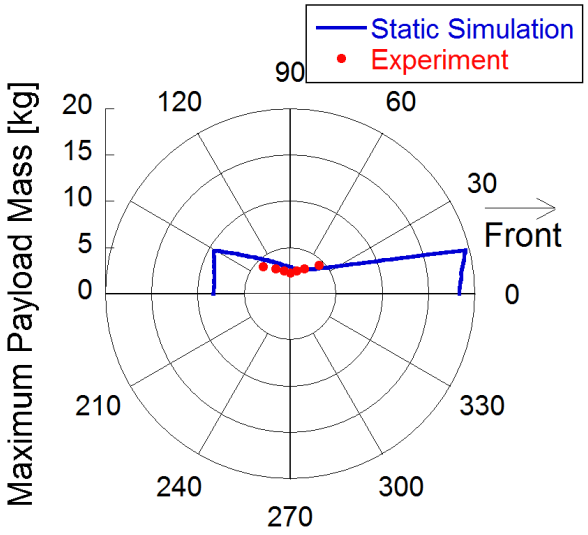

Figure 91: Comparison of simulation and experimental results of maximum static payload mass for a base width of 0.43 meters.

Figure 92 shows the maximum static payload mass for a base width of 0.33 meters and experimental points at certain slew angles. Experimental results are similar to simulation results.

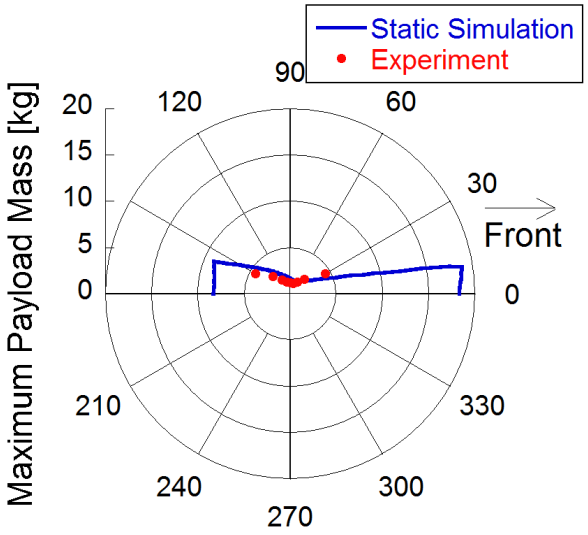

Figure 92: Comparison of simulation and experimental results of maximum static payload mass for a base width of 0.33 meters.

Figure 93 shows the difference of maximum static payload mass for different base widths: 0.43, 0.38, 0.33, 0.28 meters. As the base width decreases the maximum static payload mass at the same slew angles decreases.

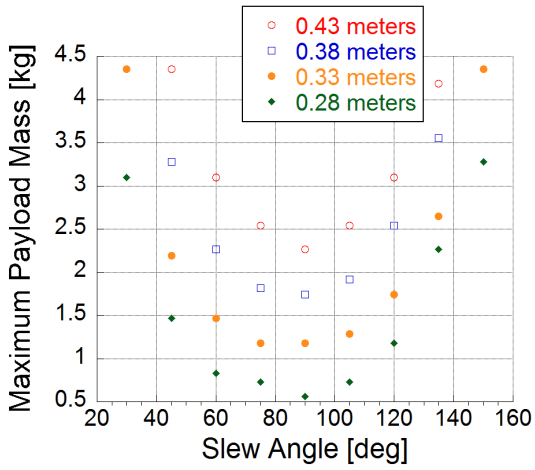

Figure 93: Comparison of experimental results of maximum static payload mass for different base widths.

4.4 Summary

An increase in platform mass, decreases the tip-over stability margin. Overcenter configurations have greater stability and less residual amplitude than their counterpart non-overcenter configurations. Strategically choosing overcenter configurations is a way operators can increase the aerial lift's tip-over stability margin. A decrease in base width decreases the maximum static payload mass.

CHAPTER V

CONCLUSIONS AND FUTURE WORK

5.1 Conclusions

Aerial lifts and their dynamics were studied in this thesis. Aerial lifts are used by many to reach high heights. Aerial lifts are used on construction sites, for window washings, clearing debris from storms, repairing electrical lines, and even on movie sets. There are many different aerial lifts. They can be classified into six types that effectively describe their kinematics. Oscillations and tip-over of aerial lifts are some of the currently least controlled hazards of working on aerial lifts.

Full-size aerial lifts, a scissor lift and articulating aerial lift, were investigated for their oscillation inducing movements. Oscillations are induced by both machine and operator movements. More oscillation resulted on the articulating aerial lift than the scissor lift.

A dynamic model of an articulating aerial lift was created to study the dynamics of an articulating aerial lift in great detail. Oscillation simulations showed overcenter configurations reduce residual amplitude. Residual amplitude for slewing moves quickly plateau. Two-mode residual amplitude effect appeared for an extended configuration and slewing moves. From studying the residual oscillation of slewing and combined slewing and elbow luffing moves, an oscillation frequency and damping ratio for the model articulating aerial lift were calculated to form an input shaper. Input shaping reduced residual amplitude for slewing moves as well as slewing and elbow luffing moves.

A dynamic tip-over stability of the model articulating aerial lift was studied. Oscillation in the dynamic model articulating aerial lift was shown to decrease the tip-over stability margin compared to the static tip-over margin. By increasing the platform mass for the same configuration, the tip-over stability margin decreased. Non-overcenter and overcenter configurations with the same platform end location were presented. Tip-over

stability margin of the overcenter configurations showed greater stability than the corresponding non-overcenter configurations. Maximum residual amplitude was also smaller for overcenter configurations than the corresponding non-overcenter configurations.

5.2 Future Work

From the categorization, simulations, and experiments in this thesis, future work in the area of aerial lifts have a better direction to investigate certain aerial lifts that propose greater risks in order to help eliminate or reduce some of those hazards.

Other possible investigation of simulations to conduct are applying different input shapers to the model articulating aerial lift and comparing their settling time and the unshaped settling time. In addition, comparison of maximum residual amplitudes for each shaper can be included to determine better suited controllers for articulating aerial lifts.

Experimental trials on the model articulating aerial lift should be conducted to compare to oscillation results. In addition, the model aerial lift can be given shaped inputs to compare to shaped simulation results.

Finally, articulating aerial lifts have two joints that induce two-mode oscillations. For future work, methods of decreasing the effects form the multiple joints by two-mode input shapers can be studied and factored into choosing the best suited controller for articulating aerials lifts.

APPENDIX A

STATIC STABILITY MOTION GENESIS CODE

Chapter 4's static stability analysis used the following Motion Genesis code, created by Dr. Joshua Vaughan and Dr. William Singhose, to simulate the aerial lift under investigation.

```
% Define Newtonian Frame
NewtonianFrame  N

% Define arms as rigid bodies
RigidBody FixedBase  % Non-moving portion of Platform Base
RigidBody Base % Platform Base
RigidBody A % Lower Outer Arm
RigidBody B % Lower Inner Arm
RigidBody C  % Connector link - remains vertical
RigidBody D    % Upper Outer Arm
RigidBody E  % Upper Inner Arm
RigidBody F % Basket Arm
RigidBody G % Basket and Connector

% Define cherry picker bucket load as a point mass
Particle M

% Define points - for plotting position of links in MATLAB
Point LAstart(A), LAend(A)
Point LBstart(B), LBend(B)
Point LCstart(C), LCend(C)
Point LDstart(D), LDend(D)
Point LEstart(E), LEend(E)
Point LFstart(F), LFend(F)
Point LGstart(G), LGend(G)

% Specify Arm Lengths
Constant LA, LB, LC, LD, LE, LF, LG

% Base(s) properties
Constant Lbase  % rotating base length
Constant Hbase % rotating base height
Constant Lfixed  % fixed base length
Constant Wfixed  % fixed base width
Constant Hfixed  % fixed base height
```

```
% Set Interia Properties
FixedBase.SetMass(mFixedBase)
Base.SetMass(mBase)
A.SetMass(mA)
B.SetMass(mB)
C.SetMass(mC)
D.SetMass(mD)
E.SetMass(mE)
F.SetMass(mF)
G.SetMass(mG)
M.SetMass(mM)

FixedBase.SetInertia(FixedBasecm, Ifixx, Ifixy, Ifixz)
Base.SetInertia(Basecm, Ibasex, Ibasey, Ibasez)
A.SetInertia(Acm, IAx, IAy, IAz)
B.SetInertia(Bcm, IBx, IBy, IBz)
C.SetInertia(Ccm, ICx, ICy, ICz)
D.SetInertia(Dcm, IDx, IDy, IDz)
E.SetInertia(Ecm, IEx, IEy, IEz)
F.SetInertia(Fcm, IFx, IFy, IFz)
G.SetInertia(Gcm, IGx, IGy, IGz)

% Variables of Interest
Specified theta''% Rotation angle of base
Specified thetaL''  % angle of lower arms
Specified thetaU''% angle of upper arms
Specified thetaB''% angle of basket arm (Lf)
Specified delLow''% extension of lower arm
Specified delUp''% extension of upper arm

%----- Rotational kinematics
% Rotations - defines angular velocities and accelerations
Base.RotateZ(N, theta)
A.RotateX(Base, -thetaL)
B.RotateX(Base, -thetaL)
D.RotateX(Base, thetaU)
E.RotateX(Base, thetaU)
F.RotateX(Base, -thetaB)
G.RotateZ(N, theta)

% Enter location of body COMs - defines velocities and accelerations
FixedBasecm.Translate(No, 0>)
Basecm.Translate(No, Hbase/2*Nz>)
P_No_LAstart> = Lbase/2*Basey> + Hbase*Basez>

Acm.Translate(No, P_No_LAstart> - LA/2*Ay>)
Bcm.Translate(No, P_No_LAstart> - (delLow + LB/2)*Ay>)
Ccm.Translate(No, P_No_LAstart> - (delLow + LB)*Ay> + Lc/2*Nz>)
```

```
Dcm.Translate(No, P_No_Ccm> + LC/2*Nz> + LD/2*Dy>)
Ecm.Translate(No, P_No_Ccm> +LC/2*Nz> + (delUp + LE/2)*Dy>)
Fcm.Translate(No, P_No_Ecm> + LE/2*Ey> + LF/2*Fy>)
Gcm.Translate(No, P_No_Fcm> + LG/2*Gy>)

% Locate bucket load (person + gear) COM in Newtonian frame
M.Translate(No, P_No_Gcm> + Nz>)

%----- Define vectors to endpoints of links for plotting in MATLAB
P_No_LAend> = P_No_LAstart> -LA*Ay>
P_No_LBstart> = P_No_LAstart> - delLow*Ay>
P_No_LBend> = P_No_LBstart> - LB*Ay>
P_No_LCstart> = P_No_LBend>
P_No_LCend> = P_No_LCstart> + LC*Nz>
P_No_LDstart> = P_No_LCend>
P_No_LDend> = P_No_LDstart> + LD*Dy>
P_No_LEstart> = P_NO_LCend> + delUp*Dy>
P_No_LEend> = P_No_LEstart> + LE*Dy>
P_No_LFstart> = P_No_LEend>
P_No_LFend> = P_No_LFstart> + LF*Fy>
P_No_LGstart> = P_No_LFend>
P_No_LGend> = P_No_LGstart> + LG*Ny>

%----- Express endpoints in the Newtonian Frame
% Start of link is always the point closer to the base along the chain
Express(P_No_LAstart>,N)
Express(P_No_LBstart>,N)
Express(P_No_LCstart>,N)
Express(P_No_LDstart>,N)
Express(P_No_LEstart>,N)
Express(P_No_LFstart>,N)
Express(P_No_LGstart>,N)

% Ends are always the point farther from the base along the chain
Express(P_No_LAend>,N)
Express(P_No_LBend>,N)
Express(P_No_LCend>,N)
Express(P_No_LDend>,N)
Express(P_No_LEend>,N)
Express(P_No_LFend>,N)
Express(P_No_LGend>,N)

Express(P_No_M>,N)

% Input forces acting on sytsem
g> = -9.81*Nz>
System.AddForceGravity(g>)
```

```
%----- Get Center of Mass Location
CMPositionFromNo> = System.GetCmPosition(No)
% Express in Newtonian Frame
SysCM_x = Dot(CMPositionFromNO>,Nx>)
SysCM_y = Dot(CMPositionFromNO>,Ny>)
SysCM_z = Dot(CMPositionFromNO>,Nz>)

% Get link endpoints for plotting

% Save dynamics code for later
% Set up Kane's Method
%SetGeneralizedSpeed(thetaL',thetaU',thetaB',delLow,delUp)
%Dynamics = System.GetDynamicsKane()
%Solve(Dynamics,thetaL',thetaU',thetaB',delLow,delUp)

% Option - set up kinetic energy
% KE = System.GetKineticEnergy()
% PE = System.GetForceGravityPotentialEnergy(g>,No)
% Energy =  KE + PE

% Setup parameters to pass to Matlab Code
% Integration parameters
% Input  tFinal=10,      integStp=0.02,    absErr=1.0E-07,
%relErr=1.0E-07

% Constant values
%Input LA = 5.9 m, LB = 5.9 m, LC = 1.59 m, LD = 9.62 m, LE = 9.62 m,
%LF = 2 m, LG = 1.53 m
%Input mA = 200 kg, mB = 200 kg, mC = 200 kg, mD = 200 kg,
%mE = 200 kg, mF = 200 kg, mG = 200 kg, mM = 100 kg

% Initial conditions
%Input thetaA = 15 deg, thetaB = 15 deg, thetaA' = 0 deg/sec,
%thetaB' = 0 deg/sec

% Quantities to output
%Output t, thetaA deg, thetaB deg, thetaA deg/sec, thetaB deg/sec

% Create MATLAB code
%ODE() Cherrypicker_Telescoping.m

% Save input/output
Save CherryPickterTelescoping_dynamics.all
```

APPENDIX B

DYNAMIC MODEL OF DOUBLE-BOOM ARTICULATING AERIAL WORK LIFT AUTOLEV CODE

B.1 Background

To simulate a double-boom articulating aerial work lift, the following autolev code was used. From this code Autolev generated the equations of motion of the system shown in Chapter 3 of this thesis. In the code q's are the θ's in the equations of motion. An apostrophe denotes velocity, $\dot{\theta}$, and two apostrophes together denote acceleration, $\ddot{\theta}$. d's in front of the q's infer velocity as well. In addition, the term *damp* in the code is K_{d4}, the damping coefficient on the payload joint.

B.2 Code

```
% Newtonian, bodies, frames, points, particles
Newtonian N
Bodies T, C, Lb, Ub, B
Points TC, CS, SH, EL, UbE, COM
Particle P

% Constants
Constants g, L0, rc, LC, L1, L2, L3
Constants xcom, ycom
Constants kp1, kp2, kp3, kd1, kd2, kd3, damp

% Masses
Mass T=mT, C=m0, Lb=m1, Ub=m2, B=0, P=m3

% Inertia
Inertia C, (1/12)*m0*(3*rc^2+L0^2), (1/12)*m0*(3*rc^2+L0^2), (1/2)*m0*rc^2
Inertia Lb, 0, (1/12)*m1*L1^2, (1/12)*m1*L1^2
Inertia Ub, 0, (1/12)*m2*L2^2, (1/12)*m2*L2^2
Inertia B, 0, 0, 0

% Variables
Motionvariables' q1'', q2'', q3'', q4''
Specified q1d, q2d, q3d, dq1d, dq2d, dq3d
```

```
% Rotation of frames
N_T = Diagmat(3,1)
Simprot (T, C, 3, q1)
Simprot (C, Lb, 2, -q2)
Simprot (Lb, Ub, 2, q3)
Simprot (Ub, B, 2, q4+q2-q3)

% Position vectors
P_NO_TC> = 0>
P_NO_TO> = -xcom*T1> + ycom*T2>
P_NO_CS> = -LC*T1>
P_CS_SH> = L0*C3>
P_CS_CO> = (1/2)*L0*C3>
P_SH_EL> = L1*Lb1>
P_SH_LbO> = (1/2)*L1*Lb1>
P_EL_UbE> = -L2*Ub1>
P_EL_UbO> = -(1/2)*L2*Ub1>
P_UbE_P> = -L3*B3>
P_UbE_BO> = -(1/2)*L3*B3>

% Angular velocity
W_T_N> = 0>
W_C_N> = q1'*C3>
W_Lb_N> = W_C_N> - q2'*Lb2>
W_Ub_N> = W_Lb_N> + q3'*Ub2>
W_B_N> = W_Ub_N> + (q4'+q2'-q3')*Ub2>

% Velocities
V_TO_N> = 0>
V_CO_N> = 0>
V_SH_N> = 0>
V2pts(N, Lb, SH, LbO)
V2pts(N, Lb, SH, EL)
V2pts(N, Ub, EL, UbO)
V2pts(N, Ub, EL, UbE)
V2pts(N, B, UbE, BO)
V2pts(N, B, UbE, P)

% Angular accelerations
ALF_T_N> = 0>
ALF_C_N> = DT(W_C_N>, N)
ALF_Lb_N> = DT(W_Lb_N>, N)
ALF_Ub_N> = DT(W_Ub_N>, N)
ALF_B_N> = DT(W_B_N>, N)

% Accelerations
A_TO_N> = 0>
A_CO_N> = 0>
```

```
A_SH_N> = 0>
A2pts(N, Lb, SH, LbO)
A2pts(N, Lb, SH, EL)
A2pts(N, Ub, EL, UbO)
A2pts(N, Ub, EL, UbE)
A2pts(N, B, UbE, BO)
A2pts(N, B, UbE, P)

% Forces
Gravity (-g*N3>)
Torque_C>+=(kp1*(q1d-q1)+kd1*(dq1d-q1'))*C3>
Torque (C/Lb, (kp2*(-q2d+q2)+kd2*(-dq2d+q2'))*Lb2>)
Torque (Lb/Ub, (kp3*(q3d-q3)+kd3*(dq3d-q3'))*Ub2>)
Torque_B> = -damp*q4'*Ub2>

ZERO = FR( ) + FRSTAR( )
KANE()

UNITSYSTEM kg, meter, sec
INPUT mT=4.2 kg,m0=1 kg,m1=2 kg,m2=2 kg,m3=2 kg
INPUT ycom = 0 m, xcom = 0.04 m, LC = 0.05 m, rc = 0.025 m
INPUT L0=0.195 m, L1=1 m, L2=1 m,L3=0.05 m
INPUT kp1 = 500 N/m, kp2 = 3500 N/m, kp3 = 2000 N/m
INPUT kd1 = 20 N*sec/m, kd2 = 40 N*sec/m, kd3 = 40 N*sec/m
INPUT g=9.81 m/sec^2, TFinal = 20 sec, damp = 1.0 N*sec/m
OUTPUT T sec, q1 rad, q2 rad, q3 rad, q4 rad, q1' rad/sec,
q2' rad/sec, q3' rad/sec, q4' rad/sec, q1'' rad/sec^2,
q2'' rad/sec^2, q3'' rad/sec^2, q4'' rad/sec^2

CODE DYNAMICS() Dyn_Cherry_Picker_Sim.m

SAVE Dyn_Cherry_Picker_Sim.all
```

REFERENCES

[1] BUCKETTRUCKS.ORG, "Your authority on bucket truck information." [Online]. Available: http://www.buckettrucks.org, Date Accessed: 2/12/2012 2012.

[2] CAZZULANI, G., RESTA, F., and RIPAMONTI, F., "A feedback and feedforward vibration control for a concrete placing boom," *Journal of Vibration and Acoustics*, vol. 133, no. 5, pp. 051002–8, 2011.

[3] EQUIPMENT, M., "Manlift grove a125j." [Online]. Available: http://www.maktas.net/Grove.pdf, Date Accessed: 11/18/2011 2011.

[4] FUJIOKA, D. D., MALEKI, E., and SINGHOSE, W. E., "Tip-over stability of a cherrypicker," in *ECCOMAS Thematic Conference on Multibody Dynamics*, (Brussels, Belgium), 2011.

[5] FUJIOKA, D. D., RAUCH, A., SINGHOSE, W. E., and JONES, T., "Tip-over stability analysis of mobile boom cranes with double-pendulum payloads," in *American Control Conference (ACC)*, pp. 3136–3141, 2009.

[6] HU, H., LI, E., ZHAO, X., LIANG, Z., and YU, W., "Adaptive fuzzy sliding mode controller design for folding-boom aerial platform vehicle," in *International Conference on Robotics and Biomimetics (ROBIO)*, (Tianjin, China), pp. 1656–1661, 2010.

[7] HU, H., LI, E., ZHAO, X., LIANG, Z., and YU, W., "Modeling and simulation of folding-boom aerial platform vehicle based on the flexible multi-body dynamics," in *International Conference on Intelligent Control and Information Processing (ICICIP)*, (Dalian, China), pp. 798–802, 2010.

[8] HYDE, J. M. and SEERING, W. P., "Using input command pre-shaping to suppress multiple mode vibration," in *Robotics and Automation, 1991. Proceedings., 1991 IEEE International Conference on*, pp. 2604–2609 vol.3, 1991.

[9] JIA, H., LI, W., and SINGHOSE, W., "Using two-mode input shaping to repress the residual vibration of cherry pickers," in *Measuring Technology and Mechatronics Automation (ICMTMA), 2011 Third International Conference on*, vol. 3, pp. 1091–1094, 2011.

[10] MALEKI, E., PRIDGEN, B., XIONG, J. Q., and SINGHOSE, W. E., "Dynamic analysis and control of a portable cherrypicker," in *Dynamic Systems and Control Conference (DSCC)*, vol. 2, pp. 477–482, 2010.

[11] MALEKI, E. and SINGHOSE, W., "Dynamics and control of a small-scale boom crane," *Journal of Computational and Nonlinear Dynamics*, vol. 6, no. 3, pp. 031015–8, 2011.

[12] MALEKI, E. and SINGHOSE, W. E., "Dynamics and zero vibration input shaping control of a small-scale boom crane," in *American Control Conference (ACC)*, pp. 2296–2301, 2010.

[13] Maleki, E., Singhose, W. E., and Srinivasan, S., "Positioning and control of boom crane luffing with double-pendulum payloads," in *IEEE International Conference on Control Applications (CCA)*, pp. 1319–1324, 2010.

[14] Mitiguy, P. and Reckdahl, K., "Autolev," March 12, 2005 2005. version 4.

[15] Pan, C. S., Hoskin, A., McCann, M., Lin, M.-L., Fearn, K., and Keane, P., "Aerial lift fall injuries: A surveillance and evaluation approach for targeting prevention activities," *Journal of Safety Research*, vol. 38, no. 6, pp. 617–625, 2007.

[16] Papadopoulos, E. G. and Rey, D. A., "A new measure of tipover stability margin for mobile manipulators," in *Robotics and Automation, 1996. Proceedings., 1996 IEEE International Conference on*, vol. 4, pp. 3111–3116 vol.4, 1996.

[17] Pridgen, B., Maleki, E., Singhose, W., Seering, W., Glauser, U., and Kaufmann, L., "A small-scale cherrypicker for experimental and educational use," in *American Control Conference (ACC)*, pp. 681–686, 2011.

[18] Program, N. Y. S. D. o. H. F., "Millwright killed when aerial work platform tipped over," Fatality Assessment and Control Evaluation 03NY034, Bureau of Occupational Health, June 4, 2003 2003.

[19] Singer, N. C. and Seering, W. P., "Preshaping command inputs to reduce system vibration," *Journal of Dynamic Systems, Measurement, and Control*, vol. 112, no. 1, pp. 76–82, 1990.

[20] Yuan, Q., Lew, J., and Piyabongkarn, D., "Motion control of an aerial work platform," in *American Control Conference (ACC)*, (St. Louis, MO, USA), pp. 2873–2878, 2009.

[21] Zimmert, N., Pertsch, A., and Sawodny, O., "2-dof control of a fire-rescue turntable ladder," *IEEE Transactions on Control Systems Technology*, vol. PP, no. 99, pp. 1–15, 2011.